NASA TECHNICAL NOTE

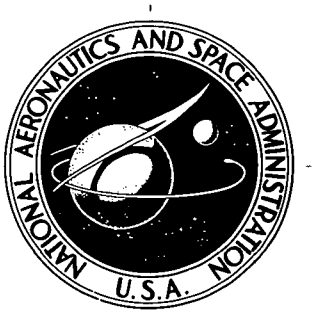

N73-24868
NASA TN D-7247

NASA TN D-7247

CASE FILE
COPY

EFFECTS OF CERTAIN CONTROL-SYSTEM NONLINEARITIES ON STABILITY AND POINTING OF AN ATTACHED DOUBLE-GIMBAL EXPERIMENT PACKAGE IN PRESENCE OF RANDOM CREW-MOTION DISTURBANCES

by John D. Shaughnessy, Nelson J. Groom, and Vilas D. Nene

Langley Research Center
Hampton, Va. 23665

NATIONAL AERONAUTICS AND SPACE ADMINISTRATION • WASHINGTON, D. C. • MAY 1973

1. Report No.	2. Government Accession No.	3. Recipient's Catalog No.
NASA TN D-7247		

4. Title and Subtitle	5. Report Date
EFFECTS OF CERTAIN CONTROL-SYSTEM NONLINEARITIES ON STABILITY AND POINTING OF AN ATTACHED DOUBLE-GIMBAL EXPERIMENT PACKAGE IN PRESENCE OF RANDOM CREW-MOTION DISTURBANCES	May 1973
	6. Performing Organization Code

7. Author(s)	8. Performing Organization Report No.
John D. Shaughnessy, Nelson J. Groom, and Vilas D. Nene*	L-7899
	10. Work Unit No. 502-23-44-02
9. Performing Organization Name and Address	11. Contract or Grant No.
NASA Langley Research Center Hampton, Va. 23665	
	13. Type of Report and Period Covered
12. Sponsoring Agency Name and Address	Technical Note
National Aeronautics and Space Administration Washington, D.C. 20546	14. Sponsoring Agency Code

15. Supplementary Notes

* NRC-NASA Resident Research Associate

16. Abstract

The effects of two types of control-system nonlinearities, sensor deadband and actuator breakout torque, on the pointing capability of an Apollo Telescope Mount (ATM) double-gimbal experiment isolation and control system are investigated. A composite structural model of a flexible experiment package connected through frictionless double gimbals to a flexible carrier vehicle is used for this investigation. Contributions of the primary carrier control system to experiment pointing are neglected. Pointing errors onboard the experiment package due to random crew-motion input into the carrier vehicle are computed. A stability investigation is performed to verify control-system stability with nominal nonlinearities and gains. Indications are that there is no stability problem due to the nonlinearities. A nonlinearity sensitivity study is carried out to determine the effects on pointing accuracy. Its results indicate that nominal ATM control system nonlinearities limit the pointing accuracy to approximately 0.4 arc second in the presence of crew motion. Methods of reducing the error to less than 0.1 arc second are discussed.

17. Key Words (Suggested by Author(s))	18. Distribution Statement
Stability and pointing of experiment package Control system nonlinearities Crew-motion disturbances	Unclassified – Unlimited

19. Security Classif. (of this report)	20. Security Classif. (of this page)	21. No. of Pages	22. Price*
Unclassified	Unclassified	43	$3.00

*For sale by the National Technical Information Service, Springfield, Virginia 22151

EFFECTS OF CERTAIN CONTROL-SYSTEM NONLINEARITIES ON STABILITY AND POINTING OF AN ATTACHED DOUBLE-GIMBAL EXPERIMENT PACKAGE IN PRESENCE OF RANDOM CREW-MOTION DISTURBANCES

By John D. Shaughnessy, Nelson J. Groom,
and Vilas D. Nene*
Langley Research Center

SUMMARY

The effects of two types of control-system nonlinearities, sensor deadband and actuator breakout torque, on the pointing capability of an Apollo Telescope Mount (ATM) double-gimbal experiment isolation and control system are investigated. A composite structural model of a flexible experiment package connected through frictionless double gimbals to a flexible carrier vehicle is used for this investigation. Contributions of the primary carrier control system to experiment pointing are neglected. Pointing errors onboard the experiment package due to random crew-motion input into the carrier vehicle are computed. A stability investigation is performed to verify control-system stability with nominal nonlinearities and gains. Indications are that there is no stability problem due to the nonlinearities. A nonlinearity sensitivity study is carried out to determine the effects on pointing accuracy. Its results indicate that nominal ATM control system nonlinearities limit the pointing accuracy to approximately 0.4 arc second in the presence of crew motion. Methods of reducing the error to less than 0.1 arc second are discussed.

INTRODUCTION

The Skylab mission is the first earth-orbiting manned laboratory in which large-scale astronomy experiments are performed. The Skylab mission stabilization requirements are that the laboratory (fig. 1) maintain an inertial hold during experiment periods and that the Apollo Telescope Mount (ATM) experiment package (fig. 2) attached to the laboratory through flex-pivot gimbals maintain a sun-oriented hold to within 2.5 seconds of arc in pitch and yaw. Skylab is the forerunner of more sophisticated space astronomy programs which will include 1- and 3-meter diffraction-limited telescopes. The 1- and

---

* NRC-NASA Resident Research Associate.

3-meter astronomy mission stabilization requirements are more stringent than those for the ATM, being better than 0.1 second of arc for the 1-meter class and 0.01 second of arc for the 3-meter class.

Several studies have been performed to determine the accuracy which can be obtained with telescopes attached to manned carrier vehicles and controlled separately. An analysis of a linear model of the Skylab experiment control system conducted by the Space Support Division of Sperry Rand Corporation under contract to George C. Marshall Space Flight Center has shown that the experiment package can be stabilized to approximately 1 second of arc in the presence of deterministic crew motions. P. G. Smith (ref. 1) considers an analytical investigation of the pointing accuracy of an orbiting gimbal-mounted telescope of the Skylab type. A rigid-telescope—flexible-carrier structural model is used. Smith concludes that the current Skylab experiment pointing system allows a pointing error of less than 0.1 second of arc in the presence of crew motion and that most of this error is caused by breakout torque in the gimbal torque motors. Means are discussed for reducing breakout torque and other sources of error to the extent that pointing errors not exceeding 0.01 second of arc are attainable with a gimbaled isolation and control system. Smith in a later study (ref. 2) considers the pointing errors induced in a flexible telescope caused by motions of the support. Smith suggests that a study be performed to determine the deformation due to random crew motion as well as the effect of the telescope attitude-control system on deformation. Reference 3 by Groom et al. includes an analysis of a linear model of the Skylab experiment control system where an analytical modal model of the flexible ATM connected by gimbals to the flexible Skylab is formulated and used. This analysis shows that in the presence of random crew motion, pointing stability to 0.1 second of arc can be achieved under ideal (linear) conditions.

The purpose of the present analysis is to extend the work performed in reference 3 to include nonlinearities in the sensors and gimbal actuators. This analysis uses computer simulation techniques to determine the control-system stability and pointing errors of the Skylab astronomy experiments caused by sensor and actuator nonlinearities in the experiment pointing control system in the presence of crew motion in the Skylab. The simulation specifically includes (a) an analytical modal model of the flexible ATM connected by gimbals to a preliminary version of the flexible Skylab, (b) nonlinear analytical models of the attitude and rate sensors with deadbands and actuators with breakout torques for the ATM pointing system, and (c) stochastic crew-motion time histories as primary disturbance inputs into the Skylab structure. No primary attitude control of the Skylab is included. Total, as well as pitch and yaw, pointing errors of the ATM are computed on a three-sigma basis. An appendix describes the method employed to develop the structural model used in this paper.

SYMBOLS

$\{d\}$	vector of structural element translations and rotations
$\{E\}$	vector of crew motion and control forces and torques
$\overline{H}(s)$	generalized crew-motion transfer function
H_S	fine-sun-sensor gain
$[I]$	identity matrix
K_aK_m	torque-motor gain
K_{rg}	rate-gyro gain
L_{tm}	torque-motor limit
$\{Q\}$	Laplace transform of $\{q\}$
$\{q\}$	vector of modal deflections
s	Laplace variable
T_b	torque motor breakout torque
$[U]$	modal matrix for carrier-telescope structure
$[UD]$	modal participation matrix
$[UF]$	modal distribution matrix
X_C,Y_C,Z_C	carrier axes
X_T,Y_T,Z_T	telescope axes
ΔG	rate-gyro deadband
ΔS	fine-sun-sensor deadband

ζ	structural damping ratio
θ	angular error
θ_y	angular error about Y_T axis
θ_z	angular error about Z_T axis
ρ_g	rate-gyro damping ratio
ρ_1, ρ_2	damping ratios in crew-motion filters
σ	standard deviation
τ_a	torque-motor time constant
τ_s	fine-sun-sensor time constant
τ_1	time constant in crew-motion filters
$\overline{\omega}_1, \overline{\omega}_2$	natural frequencies in crew-motion filters
ω_g	rate-gyro natural frequency
ω_n	natural frequencies for structural modes

Notation:

$[\ ]$	rectangular matrix
$[\cdot]^T$	transpose of $[\ ]$
$[\ ]$	diagonal matrix
$\{\ \}$	column vector
$[\ ]$	row vector

Dots over a symbol denote derivatives with respect to time.

ABBREVIATIONS

AM	airlock module
ATM	Apollo Telescope Mount
CMG	control-moment gyroscope
CSM	command and service module
c.m.	center of mass
FSS	fine sun sensor
LM	lunar module
MDA	multiple docking adapter
OWS	orbital workshop

DESCRIPTION OF STRUCTURAL MODEL

The preliminary Skylab configuration considered, shown in figure 1, is composed of a Saturn IV-B orbital workshop (OWS), a multiple docking adapter (MDA), a command and service module (CSM), and a modified lunar module (LM) with a rack which provides attachment points for solar panels, control-moment-gyroscope (CMG) hardware, and the ATM gimbal suspension system.

The ATM configuration considered, shown in figure 2, is composed of a double-gimbal suspension system with frictionless zero-stiffness bearings, an outer shell canister, and a cruciform spar with solar astronomy experiments, rate gyros, a sun sensor, and other equipment attached. At each gimbal pivot a torque motor is used to provide control torques for the ATM package.

The structural model is a mathematical model of the flexible ATM connected through frictionless double gimbals to the flexible Skylab carrier vehicle. The mathematical model is developed in the appendix from the composite structural model for the Skylab and ATM developed in reference 3. The resulting composite model consists of seven flexible-body modes (the frequencies ranging from 3.567 to 43.307 rad/sec) and eight rigid-body modes (six for the Skylab and two for the ATM).

The equations of motion for the structural model are based on the assumption usually made (see refs. 1, 3, and 4, for example) that the structural damping ratio ζ which is not included in the modal analysis can be added in an uncoupled sense in modal coordinates. A nominal value of 1 percent of critical damping is assumed to act on each flexible mode. The use of this value is consistent with previous analyses (for example, refs. 1, 3, and 5). Values of 0, 0.50, and 2 percent of critical are also considered in the stability analysis. This approach results in the equations of motion given as

$$\{\ddot{q}\} + 2\zeta\left[\omega_n\right]\{\dot{q}\} + \left[\omega_n^2\right]\{q\} = \left[UF\right]^T\{E\} \tag{1}$$

The vector $\{q\}$ defines the 15 modal displacements and has the form

$$\{q\}^T = \left[q_1, \ldots, q_{15}\right]$$

The diagonal matrix $\left[\omega_n\right]$ contains the modal natural frequencies and is given by

$$\left[\omega_n\right] = \begin{bmatrix} \omega_{n1} & & & 0 \\ & \omega_{n2} & & \\ & & \ddots & \\ 0 & & & \omega_{n15} \end{bmatrix}$$

The diagonal matrix $\left[\omega_n^2\right]$ contains the squares of the modal natural frequencies. The force vector $\{E\}$ has 14 elements; these elements include crew-motion forces and torques and control-system gimbal torques and reaction torques on the carrier. This vector is given by

$$\{E\}^T = \left[E_1, \ldots, E_{14}\right]$$

The 15 × 14 matrix $\left[UF\right]^T$ distributes the force vector $\{E\}$ over the 15 modes and is found by transposing the matrix $\left[UF\right]$ formed from the modal matrix of the coupled carrier-experiment system $\left[U\right]$ (from ref. 3) by retaining the 14 rows corresponding to force or torque application locations and directions and the 15 columns corresponding to the 15 modes retained. The resulting motion in carrier coordinates is given by the relation

$$\{d\} = \left[UD\right]\{q\} \tag{2}$$

where $[UD]$ is the matrix formed from $[U]$ by retaining those rows that correspond to the motion of the mass point of interest. See reference 3 for a more detailed discussion of the matrices of this section.

DESCRIPTION OF CONTROL SYSTEMS

The CMG system which provides Skylab stabilization is designed to control only the low frequency (0 to 1 Hz) spacecraft motions caused by external disturbances such as gravity gradient and aerodynamic torques. The higher frequency motions (1 to 5 Hz) caused by disturbances like crew motions are not controlled by the CMG system. (See ref. 1.) For these reasons and for conservative pointing accuracy estimates, the CMG system is not included in this analysis.

The control system considered is a nonlinear model of the ATM experiment pointing system with the roll-control system fixed (the roll system is manually controlled prior to experiment initiation). The system consists of two vernier gimbals driven by two direct-current, direct-drive torque motors per axis (see fig. 2(b)) with error signals derived from a two-axis fine sun sensor and rate gyros mounted on the experiment package. A block diagram of the overall system is presented in figure 3. Figure 3(b) shows the functional relationship for each nonlinearity and where they are included in the mathematical model. The fine-sun-sensor nonlinearity considered is the pointing resolution modeled as a deadband ΔS. In this study ΔS is allowed to take on six values: 0, 0.025, 0.050, 0.075, 0.1, and 0.15 volts (corresponding to 0, 0.16, 0.31, 0.47, 0.63, and 0.94 arc seconds with the nominal sun-sensor gain). The saturation limit used is ±14 volts. The rate-gyro nonlinearity studied is the null uncertainty modeled as a deadband ΔG. Eight values of ΔG are considered ranging from 0 to 0.0035 volt in steps of 0.0005 volt. With the nominal rate-gyro gain, this range corresponds to 0 to 0.28 arc second/second input rate in increments of 0.04 arc second/second. The rate-gyro saturation limit is ±45 volts. The gimbal torque-motor nonlinearity is a so-called breakout torque due to magnetic hysteresis and is modeled as coulomb friction at the gimbal pivots. The breakout torque level T_b considered ranges from 0 to 0.24 N-m in increments of 0.034 N-m. Torque-motor saturation limits of 9.5 N-m are used. Table I gives the nominal values of the nonlinearities and other experiment control-system parameters.

DESCRIPTION OF CREW-MOTION MODEL

The crew-motion disturbance model is formulated by using the method and data developed by Martin Marietta Corporation under contract to George C. Marshall Space Flight Center. The analytical method of representing single astronaut crew motion during performance of a given task is as follows: Unity power spectral density noise having

Gaussian distribution and a negligible mean is passed through linear filters to generate forces and moments statistically similar to those produced by a test subject performing the task. The method used to develop the filters is given in reference 6. The filters are included in the system block diagram in figure 3 and have the following form:

$$\overline{H}(s) = \frac{\tau_1 s}{\left(s^2 + 2\rho_1\overline{\omega}_1 s + \overline{\omega}_1^{\,2}\right)\left(s^2 + 2\rho_2\overline{\omega}_2 s + \overline{\omega}_2^{\,2}\right)} \tag{3}$$

The values of the parameters for the present analysis are given in table II and are for an astronaut performing the SO56 X-ray Telescope experiment at the ATM control and display console. (This experiment is described in ref. 7.) In this activity, the astronaut is restrained by harnesses or other devices from large translational movements of his center of mass. The activity is representative of astronaut motions during other astronomy experiments. The crew-motion disturbance location is shown in figure 1 (designated AM/MDA crew location).

METHOD OF COMPUTATION

The experiment package pointing errors due to the combined effects of the control system nonlinearities, structural flexibility, and random crew motion, each discussed previously, were computed on a Control Data Corporation 6600 computer system. Simulation equations, derived from the system block diagram given in figure 3, were solved numerically for a flight time of 10 seconds. The crew-motion disturbance history was precomputed, stored on tape, and reused for each solution. Pointing errors onboard the ATM were computed on a three-sigma basis for various combinations of the nonlinearities. The results of the computations are presented and discussed in the next section.

RESULTS AND DISCUSSION

Control System Stability

An investigation was performed to verify that the control system being considered is asymptotically stable with the nominal ATM torque-motor gain (K_aK_m), and to determine the pointing-error sensitivity to structural damping ζ. Because of the control system nonlinearities, conventional stability criteria cannot be used; therefore, time histories of angular motion of the fine sun sensor were computed for different values of K_aK_m and ζ. The results of these simulations are summarized in figures 4 to 6. The linear system is considered first for comparison with the results of reference 3. Figure 4 shows the Y_T-axis, Z_T-axis, and total three-sigma angle-pointing error as a function of torque motor gains for four different values of structural damping with the linear control system.

For each value of damping, the angular motion diverges for K_aK_m greater than 68 N-m/V. The results for the cases with a damping ratio of 0.01 agree well with those of reference 3 and indicate that the truncated structural model is adequate for the nonlinear analysis.

Figures 5 and 6 show the Y_T-axis, Z_T-axis, and total three-sigma angle-pointing errors as a function of torque-motor gain for the four values of structural damping with the nominal values of control system nonlinearities included. The total three-sigma angle-pointing errors for the linear system are included in figure 6 for reference. It is noted that the pointing errors increase as much as 30 times when the nominal nonlinearities are introduced.

An interesting phenomenon is seen on the Y_T-axis (fig. 5(a)) and total error (fig. 6) plots. For gains between 13.6 and 111.9 N-m/V, the errors decrease as damping decreases; whereas the linear system results show that the errors increase as damping decreases. Limit cycles occur above gains of 109 N-m/V for zero damping and above 122 N-m/V for damping ratios of 0.005 and 0.01. No limit cycles develop below a gain of 135.6 N-m/V for the case with damping of 0.02. For the Y_T-axis and total angle cases between gains of 27.1 and 111.9 N-m/V, a damping ratio of 0.01 gives the largest errors. The limit cycles that occur develop after several seconds of motion and result in the torque motors switching between their saturation limits.

The nominal value of torque-motor gain gives adequate accuracy for ATM; however, if greater accuracy is required, the results indicate that the control-system nonlinearities will allow the gain to be increased by a factor of two or three without causing limit cycles in the control system.

Pointing Accuracy

The effects on pointing accuracy of the control-system nonlinearities considered are summarized in figures 7 to 9. Figure 7 shows the effect of sun-sensor deadband on pointing error. Because the crew-motion disturbance inputs have negligible mean values and since the simulation is done on a highly accurate digital computer, the three-sigma pointing errors are not proportional to the deadband. In practice, slight external and internal bias torques would cause the errors to follow the size of the deadband more closely. The largest errors occur with nominal nonlinearities in the rate-gyro and torque motors. Deadbands larger than 0.05 volt do not cause any further increase in the three-sigma error since the rate-gyro feedback is sufficient to keep the error less than the size of the deadband. Elimination of the breakout torque reduces the total three-sigma angle error by an order of magnitude for sun-sensor deadbands larger than 0.05 volt. With linear torque motors and linear or nonlinear rate gyros, the variation in the fine-sun-sensor deadband has a negligible effect on pointing error since the errors are within the deadband.

Figure 8 shows the effect of rate-gyro deadband on pointing error. Again, the largest errors occur with nominal nonlinearities in the fine sun sensor and torque motors. If either the fine-sun-sensor deadband or torque-motor breakout torque is eliminated, the magnitude of the rate-gyro deadband has little or no effect on the three-sigma error. The peak errors obtained at a deadband of 0.003 volt with the nonlinear fine sun sensor and linear torque motor are caused by biased motion with the deadband. It is noted that if the breakout torque or the sun-sensor deadband could be eliminated, then any rate-gyro deadband up to and including the nominal value would not cause errors greater than 0.1 arc second.

Figure 9 shows the effect of torque-motor breakout on pointing error. It is seen that pointing errors increase directly with the magnitude of the breakout torque, and thus reduction of the breakout torque should be a prime consideration in future telescope-pointing control-system design. The rate-gyro nonlinearity does not contribute significantly to pointing error when the fine sun sensor is linear; however, when the sun sensor is nonlinear, the rate-gyro deadband causes significant increases in the pointing errors.

Reduction or elimination of the torque-motor breakout torques would significantly reduce pointing errors in ATM type isolation and control system. In practice, reduction of the sun-sensor deadband would directly reduce pointing errors. This reduction could partially be accomplished by increasing the gain of the sun sensor. The ratio of sun-sensor gain to rate-gyro gain was not changed in this study and perhaps an investigation of different ratios with different torque-motor gains could lead to a significant reduction in the predicted pointing errors.

The pointing control-system nonlinearities considered have a significant effect on the pointing capability of the ATM type system. The ATM mission requires pointing to 2.5 arc seconds and this requirement appears to be attainable in the presence of crew motion. Pointing to higher accuracy, in the 0.1-arc-second range, with the ATM type system can be achieved with the basic ATM system if the actuators and attitude sensor can be improved as outlined. The rate gyro used in the nominal ATM control system appears to be adequate for 0.1-arc-second pointing tasks.

CONCLUDING REMARKS

To determine the effects of certain control-system nonlinearities and crew motion on pointing accuracy and stability of a double-gimbal experiment isolation and control system of the Apollo Telescope Mount (ATM) type, a mathematical structural model of a flexible experiment package (ATM) connected through frictionless gimbals to a flexible carrier (Skylab) is utilized.

A model of the nominal ATM experiment pointing-control system with attitude and rate sensor deadbands and actuator breakout torque nonlinearities is used. No control system for the carrier vehicle is included since its effect should be negligible. The stability of the pointing-control system is investigated for a range of torque-motor gains and structural damping ratios. The model is subjected to continuous single-astronaut crew motion, represented by a filtered random number sequence with Gaussian distribution and negligible mean, and pointing errors are computed on a three-sigma basis about the gimbal axes of the experiment package, at the fine-sun-sensor location.

The analyses performed indicate the following:

1. The ATM pointing-control system has a three-sigma pointing error of approximately 0.4 arc second. An optimization study involving the ratio of sun-sensor gain to rate-gyro gain together with the torque-motor gain could lead to improved accuracy.

2. Pointing errors vary directly with the breakout torque and sun-sensor deadband and these nonlinearities appear to be the most critical in achieving higher pointing accuracy with the ATM type system. Moderate reductions of both of these nonlinearities should reduce predicted pointing errors to less than 0.1 arc second.

3. Control-system stability in the presence of the nonlinearities considered is not a problem; in fact, the torque-motor gain can be increased by a factor of two to three over the nominal value without causing limit cycles.

4. Structural damping does not appear to be critical to either control-system stability or pointing accuracy.

Langley Research Center,
National Aeronautics and Space Administration,
Hampton, Va., April 10, 1973.

APPENDIX

STRUCTURAL MODEL

In reference 3, a method is developed to obtain a mathematical model of a manned carrier vehicle (Skylab) carrying a large telescope (ATM). This model contains the computed natural vibration modes of structural components. The method is specifically devised to use vibration modes previously computed for the carrier vehicle with the ATM experiment package considered as a rigid mass and vibration modes for the ATM considered as an elastic body attached to a rigid base. The resulting composite model consists of 107 flexible-body modes (with frequencies ranging from 0.848 to 241.422 rad/sec) and eight rigid-body modes (six for the Skylab and two for the ATM package). In the present analysis, it is desired to reduce the order of the mathematical model by neglecting the contribution of a number of modes. The method used to truncate the structural model is to determine the frequency response of the complete structural model at the fine-sun-sensor and rate-gyro locations for inputs at the crew-motion filters and to choose the dominant modes by observing the frequencies of the peak amplitudes and retaining only those modes. Figure 10 shows the response at the fine-sun-sensor and rate-gyro locations obtained with the complete structural model. Modes at 3.567, 9.847, 12.466, 13.37, 14.331, 31.444, and 43.307 rad/sec are dominant. These seven flexible body modes and the eight rigid body modes are retained and all other modes are neglected. Figure 11 shows the linear system response of the truncated model.

REFERENCES

1. Smith, P. G.: The Pointing Accuracy of an Orbiting Gimbal Mounted Telescope. TM-69-1022-2, Bellcomm, Inc., Feb. 17, 1969. (Available as NASA CR-106643.)

2. Smith, P. G.: Support Motion Induced Vibrations of an Orbiting Cassegrain Telescope. TM-70-1022-3, Bellcomm, Inc., Mar. 17, 1970. (Available as NASA CR-110093.)

3. Groom, Nelson J.; Shaughnessy, John D.; and Nene, Vilas D.: On the Stability and Pointing of an Attached Double-Gimbal Experiment Package. NASA TN D-6676, 1972.

4. Anderson, Roger A.: Fundamentals of Vibrations. Macmillan Co., c.1967.

5. Keckler, Claude R.; Kyle, Robert G.; Will, Ralph W.; and Woolley, Charles T.: Real-Time Digital-Computer-Hardware Simulation of a Spacecraft With Control-Moment-Gyroscope Stabilization. NASA TM X-2069, 1970.

6. Hendricks, T. C.; and Johnson, C. H.: Stochastic Crew Motion Modeling. J. Spacecraft & Rockets, vol. 8, no. 2, Feb. 1971, pp. 150-154.

7. George C. Marshall Space Flight Center: Scientific Experiments for the Apollo Telescope Mount. NASA TN D-5020, 1969.

TABLE I.- NOMINAL PARAMETERS OF THE ATM CONTROL SYSTEM CONSIDERED*

Fine-sun-sensor gain, H_s, V/rad	33 000
Rate-gyro gain, K_{rg}, V/rad/sec	2580
Torque-motor gain, $K_a K_m$, N-m/V	37.95
Fine-sun-sensor time constant, τ_s, sec	0.016
Torque-motor time constant, τ_a, sec	0.0032
Rate-gyro natural frequency, ω_g, rad/sec	154.88
Rate-gyro damping ratio, ρ_g	0.8
Fine-sun-sensor deadband, ΔS, V	±0.1
Rate-gyro deadband, ΔG, V	±0.002
Torque-motor breakout torque, T_b, N-m	±0.1356
Torque-motor limit, L_{tm}, N-m	±9.492

*Data contained in this table were obtained from a survey of Skylab documents.

TABLE II.- CREW-MOTION FILTER PARAMETERS

Input	Input axis	ρ_1	$\overline{\omega}_1$	ρ_2 (a)	$\overline{\omega}_2$ (a)	τ_1
Force	X_C	0.5056	4.0291	0	0	4.1091
	Y_C	.5565	2.8065	0	0	3.8489
	Z_C	.5986	4.7634	.2357	31.2563	2563.12
Moment	X_C	0.3196	4.4158	0	0	7.27
	Y_C	.4683	4.0384	0	0	12.7861
	Z_C	.5589	4.4132	0	0	2.9666

[a] If ρ_2 and $\overline{\omega}_2$ are zero, then the term $\left(s^2 + 2\rho_2\overline{\omega}_2 s + \overline{\omega}_2{}^2\right)$ is deleted from equation (3).

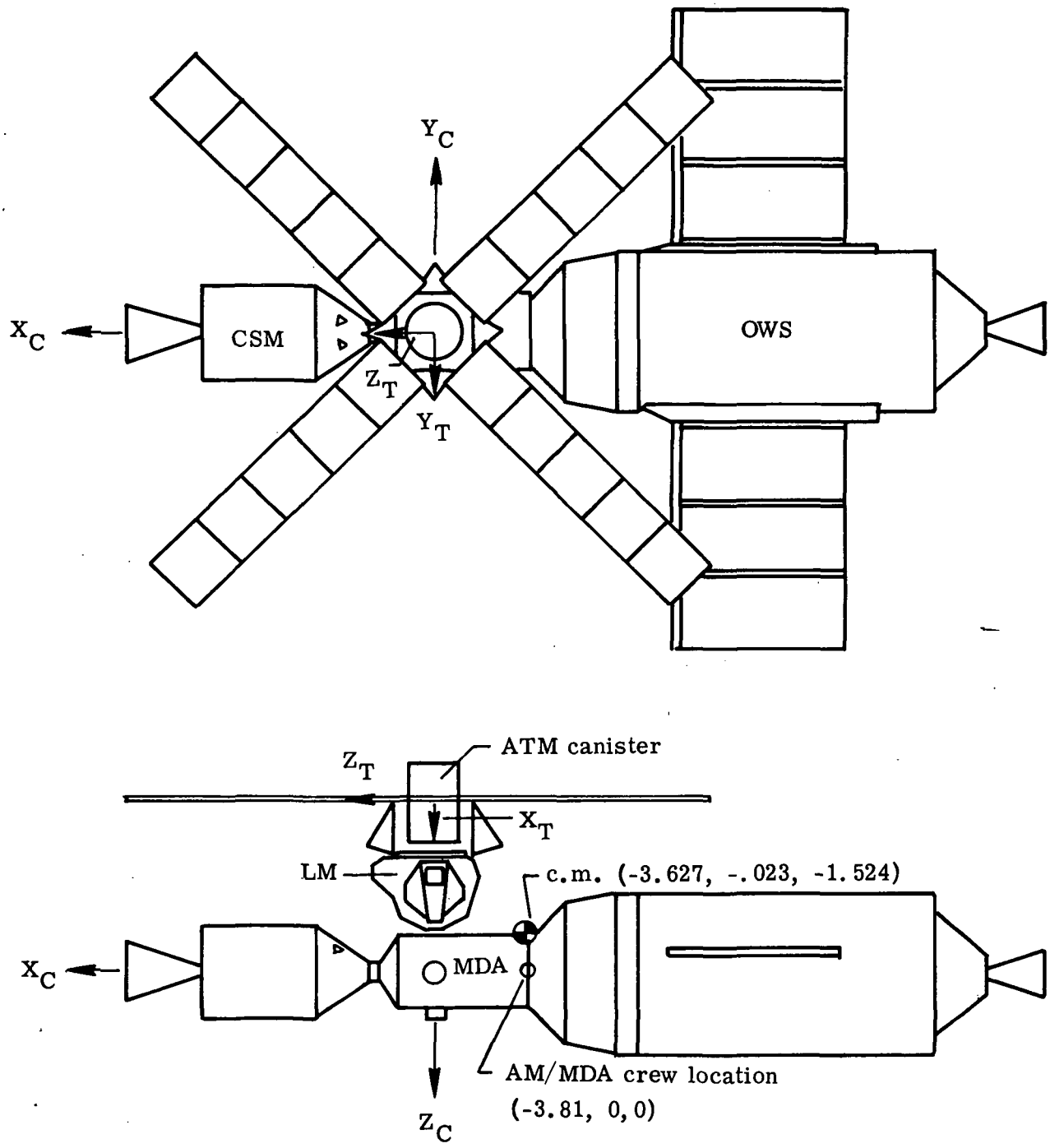

Figure 1.- Skylab configuration studied. (Numbers in parentheses are coordinates in meters with respect to the X_C, Y_C, and Z_C axes.)

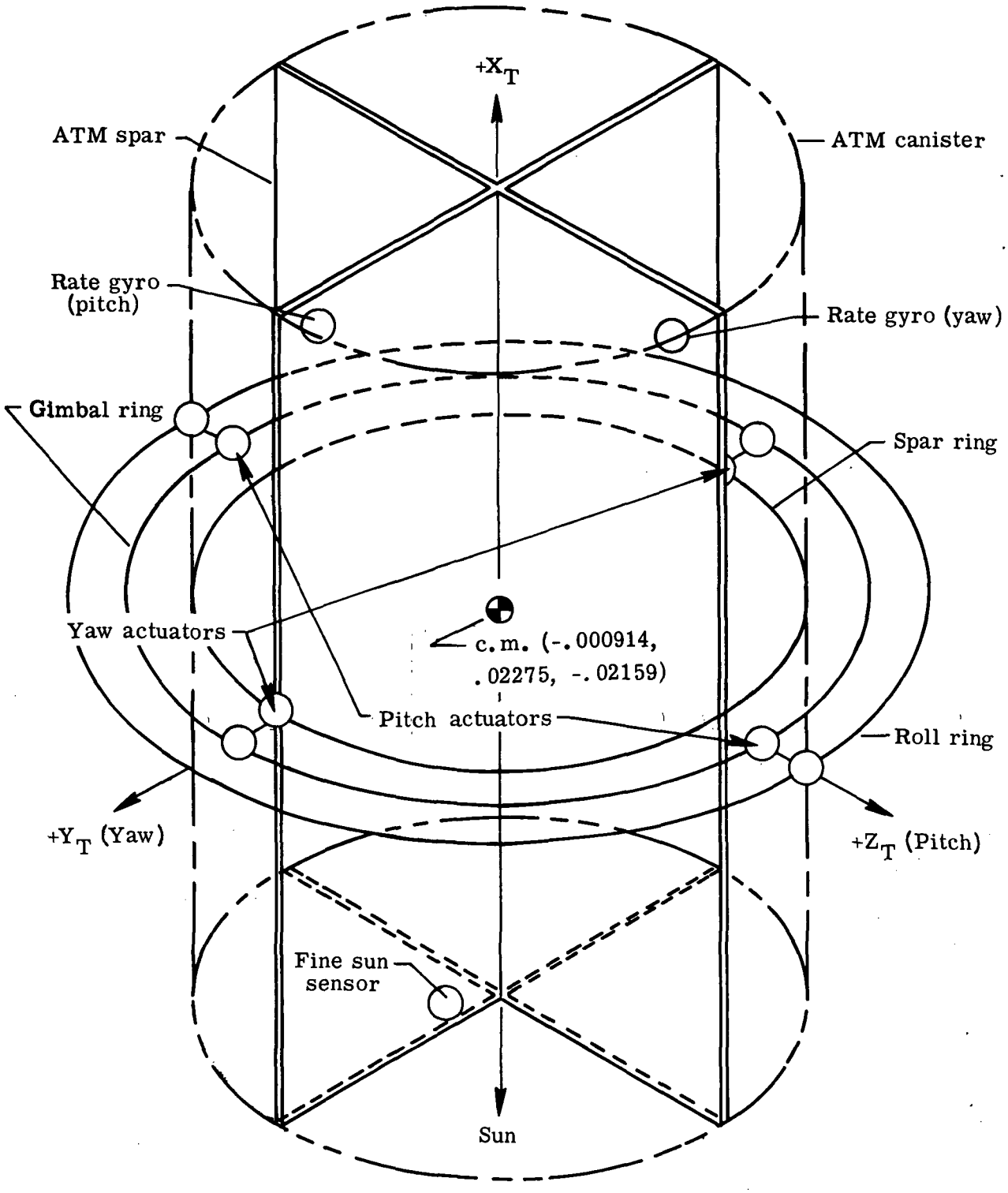

(a) Spar and ring assembly.

Figure 2.- ATM configuration (center-of-mass location is given in meters with respect to the X_T, Y_T, and Z_T axes).

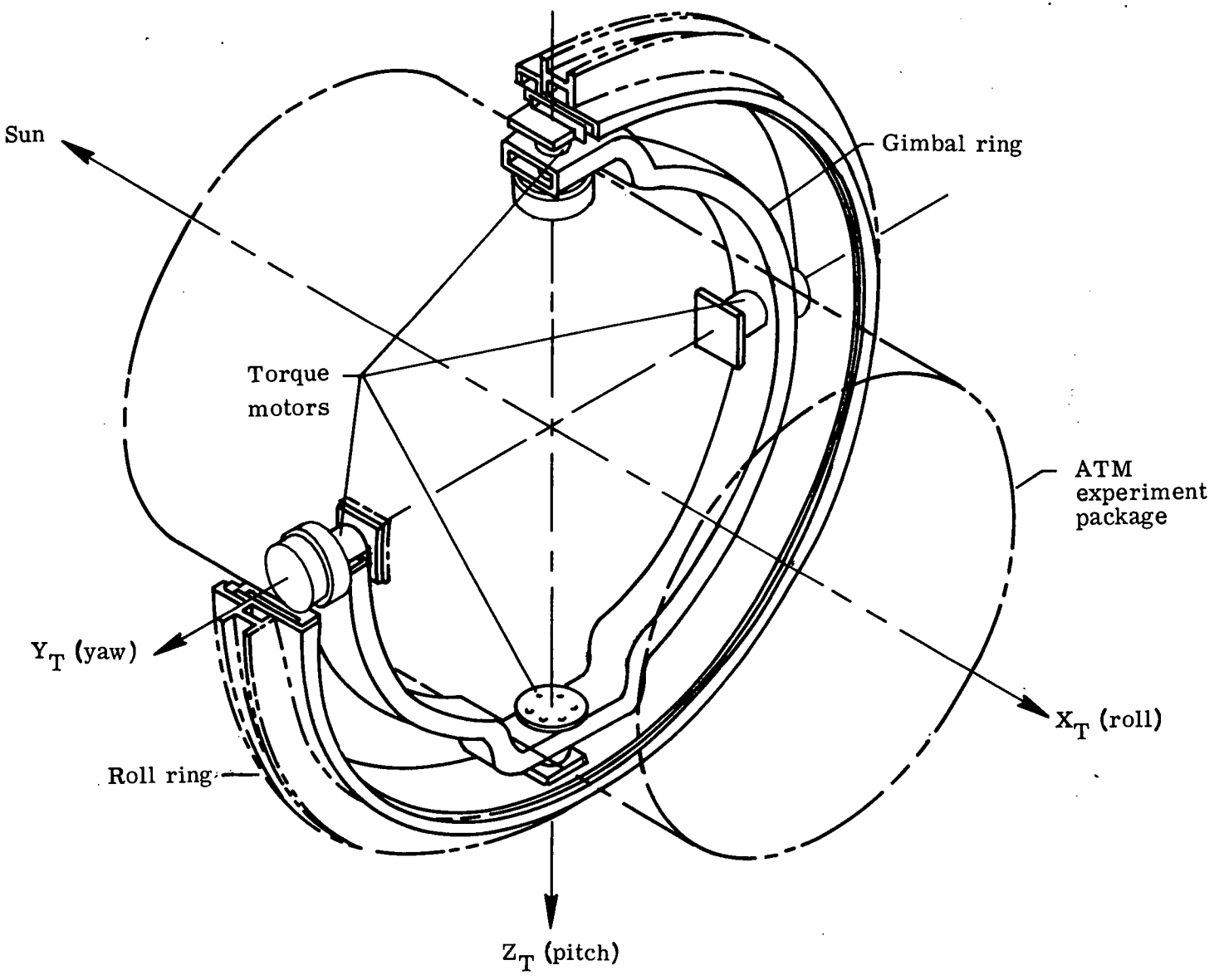

(b) Gimbal system.

Figure 2.- Concluded.

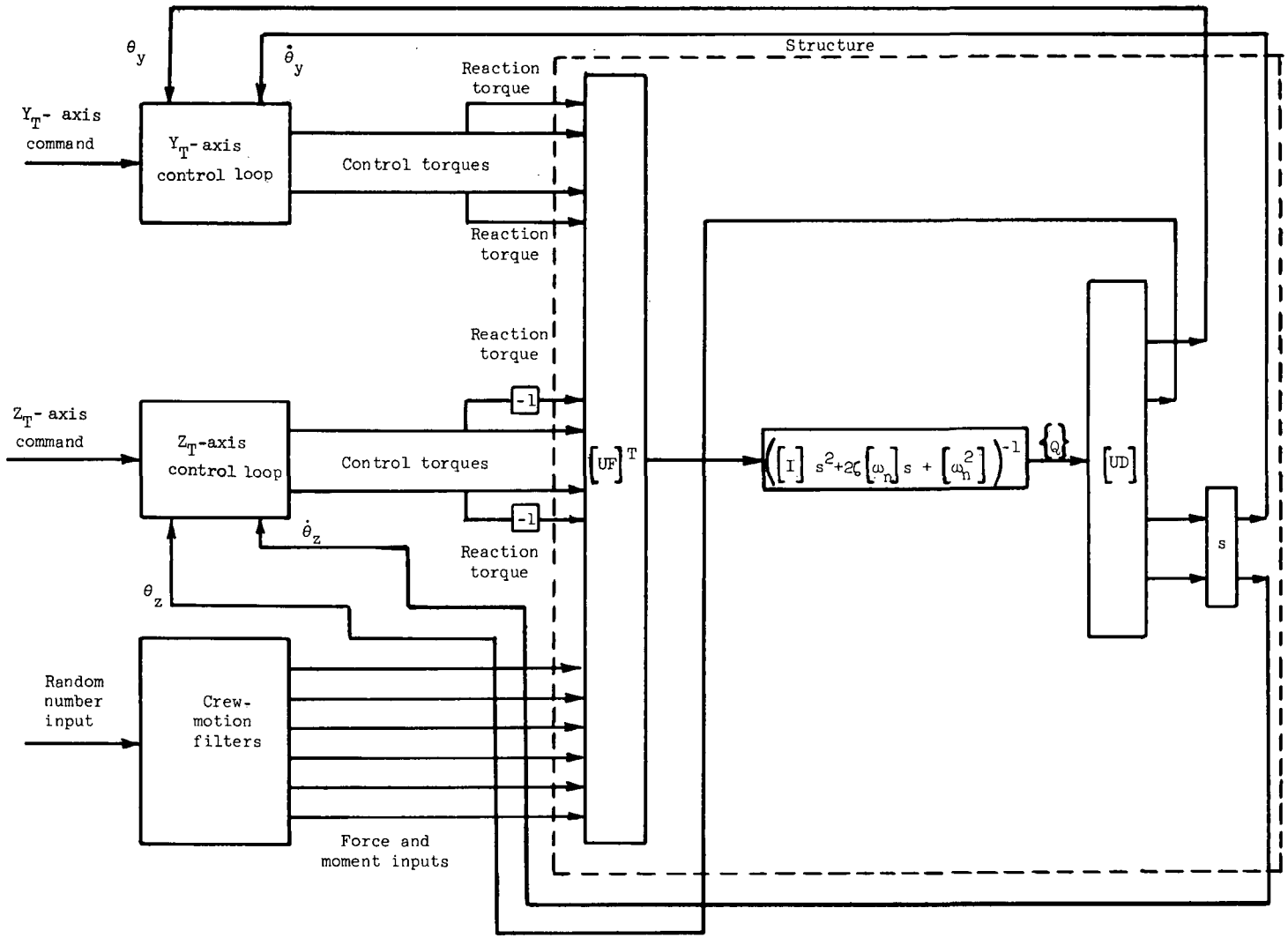

(a) Overall system.

Figure 3.- System block diagram.

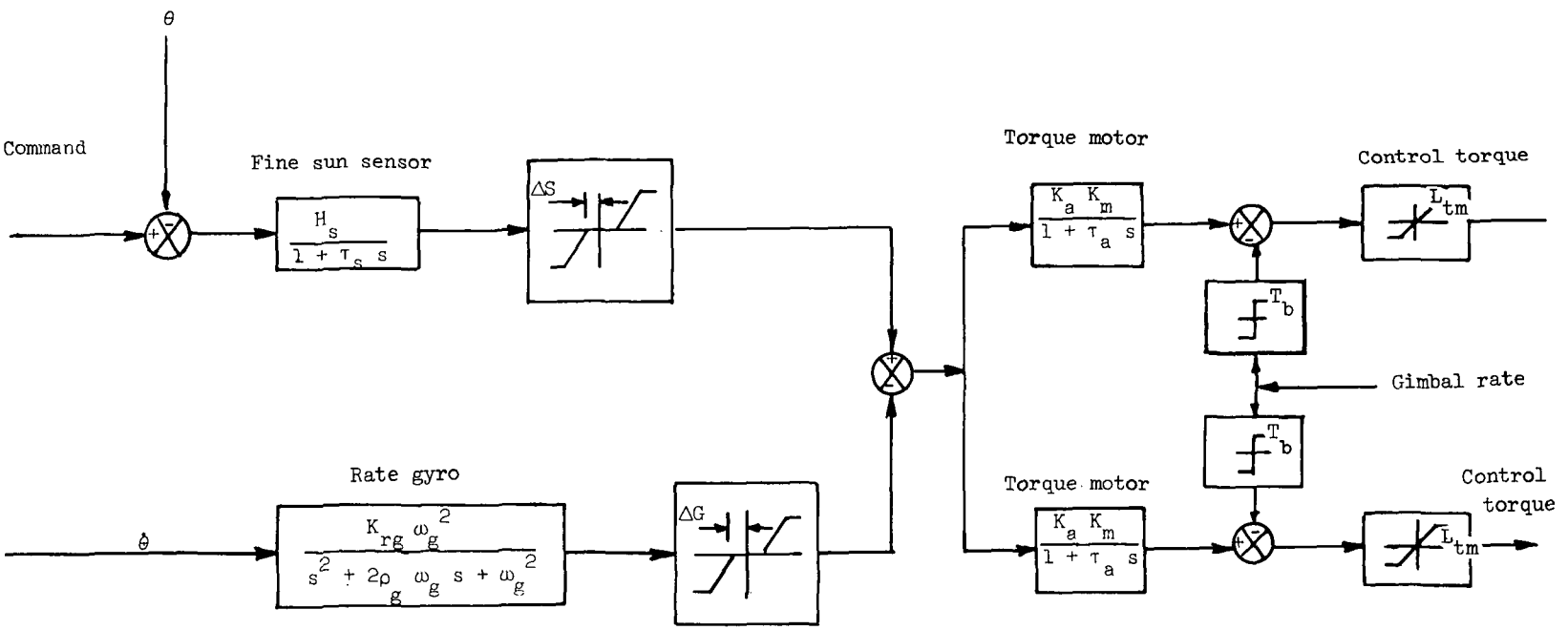

(b) Y_T- and Z_T-axis control loop.

Figure 3.- Concluded.

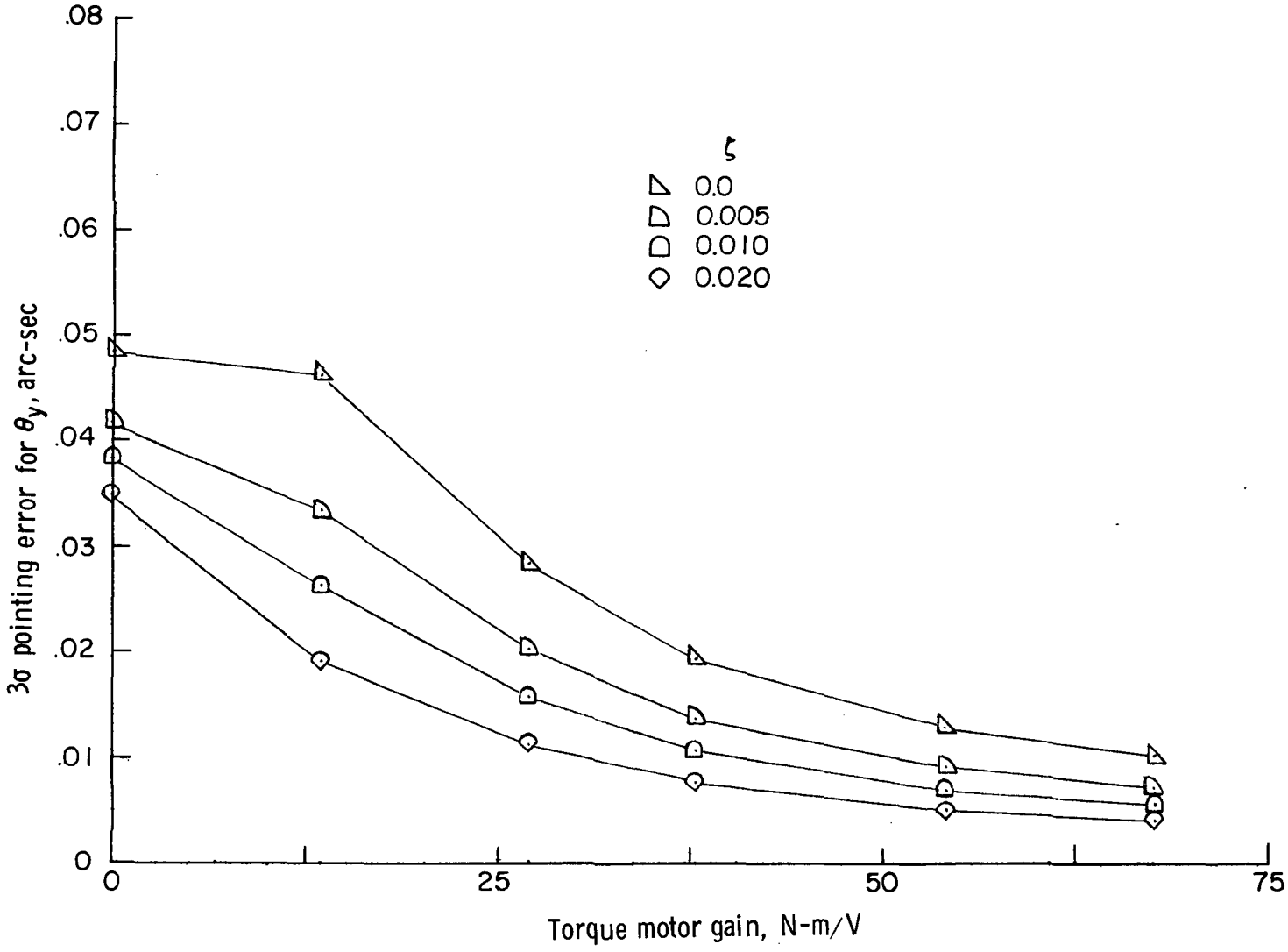

(a) Y_T-axis error.

Figure 4.- Linear-system pointing-error variation with torque motor gain.

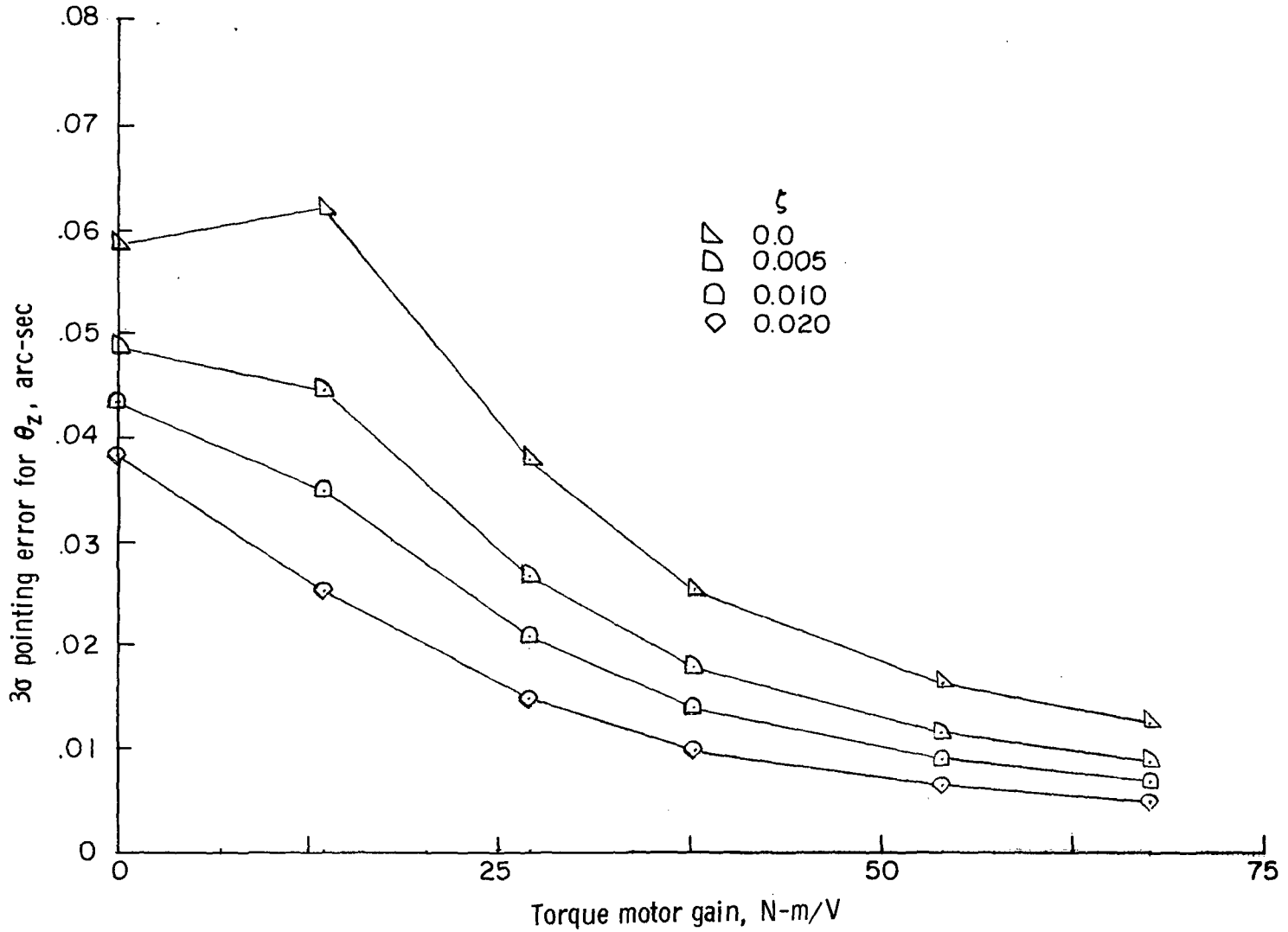

(b) Z_T-axis error.

Figure 4.- Continued.

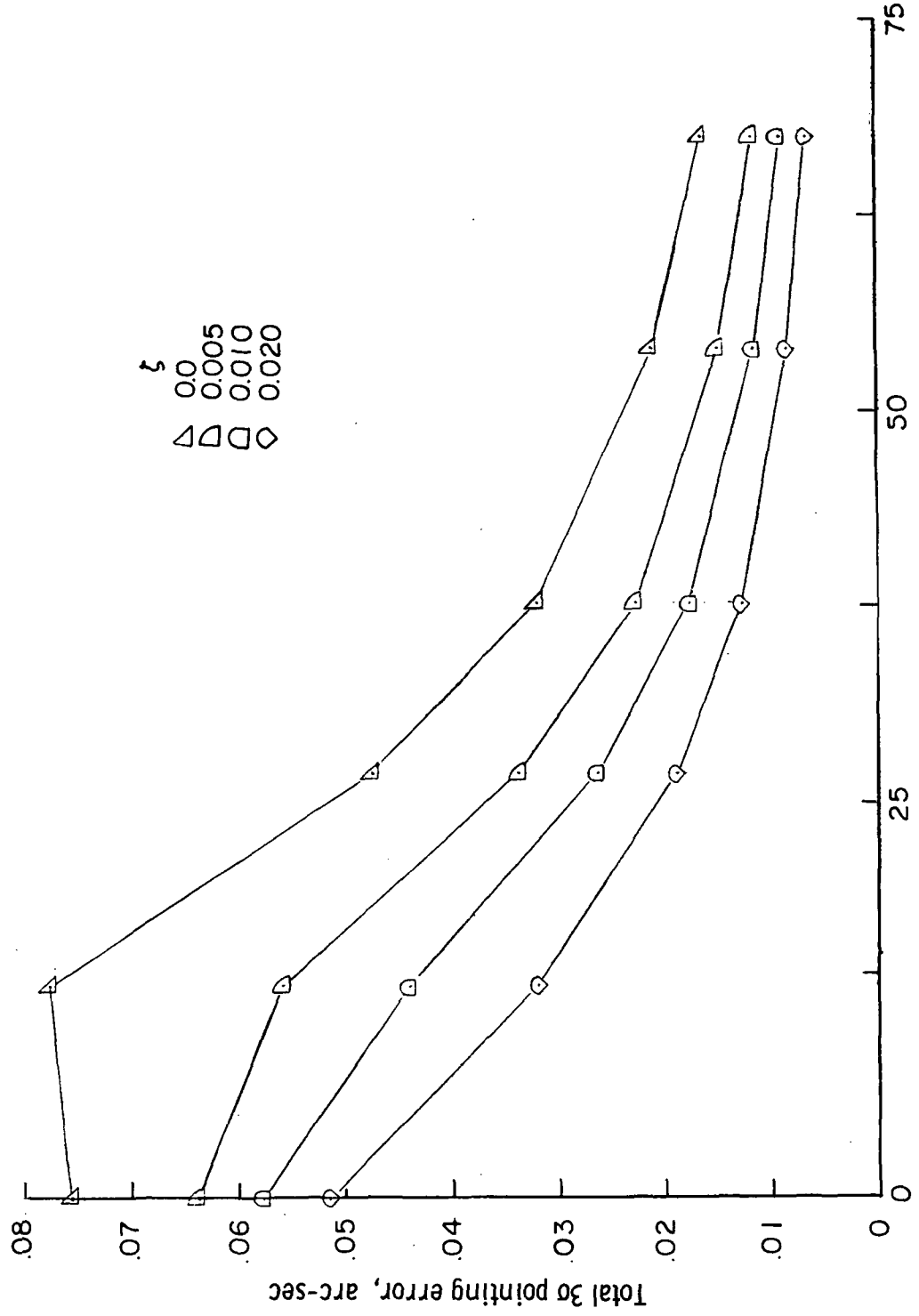

(c) Total error.

Figure 4.- Concluded.

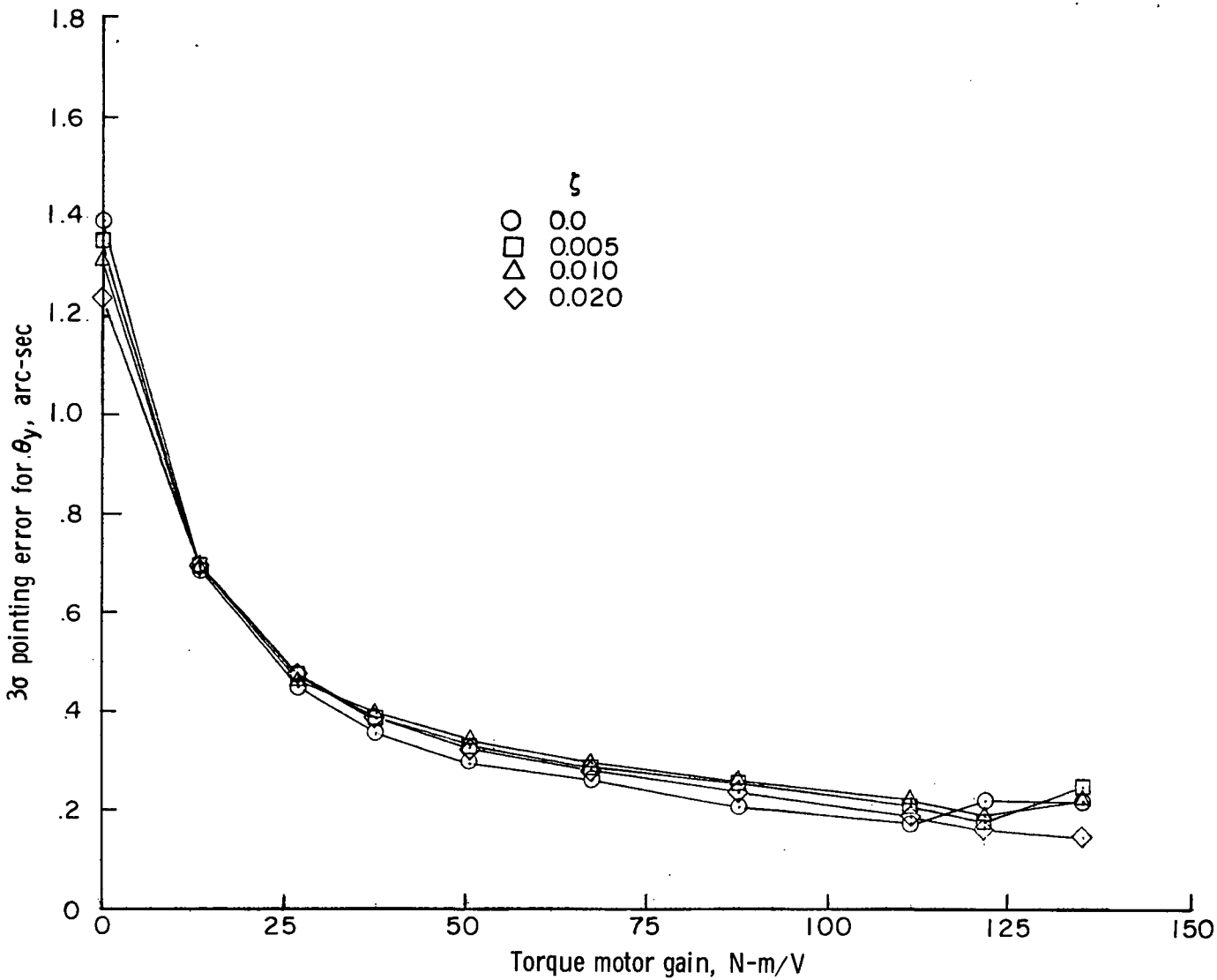

(a) Y_T-axis error.

Figure 5.- Nonlinear-system pointing-error variation with torque motor gain.

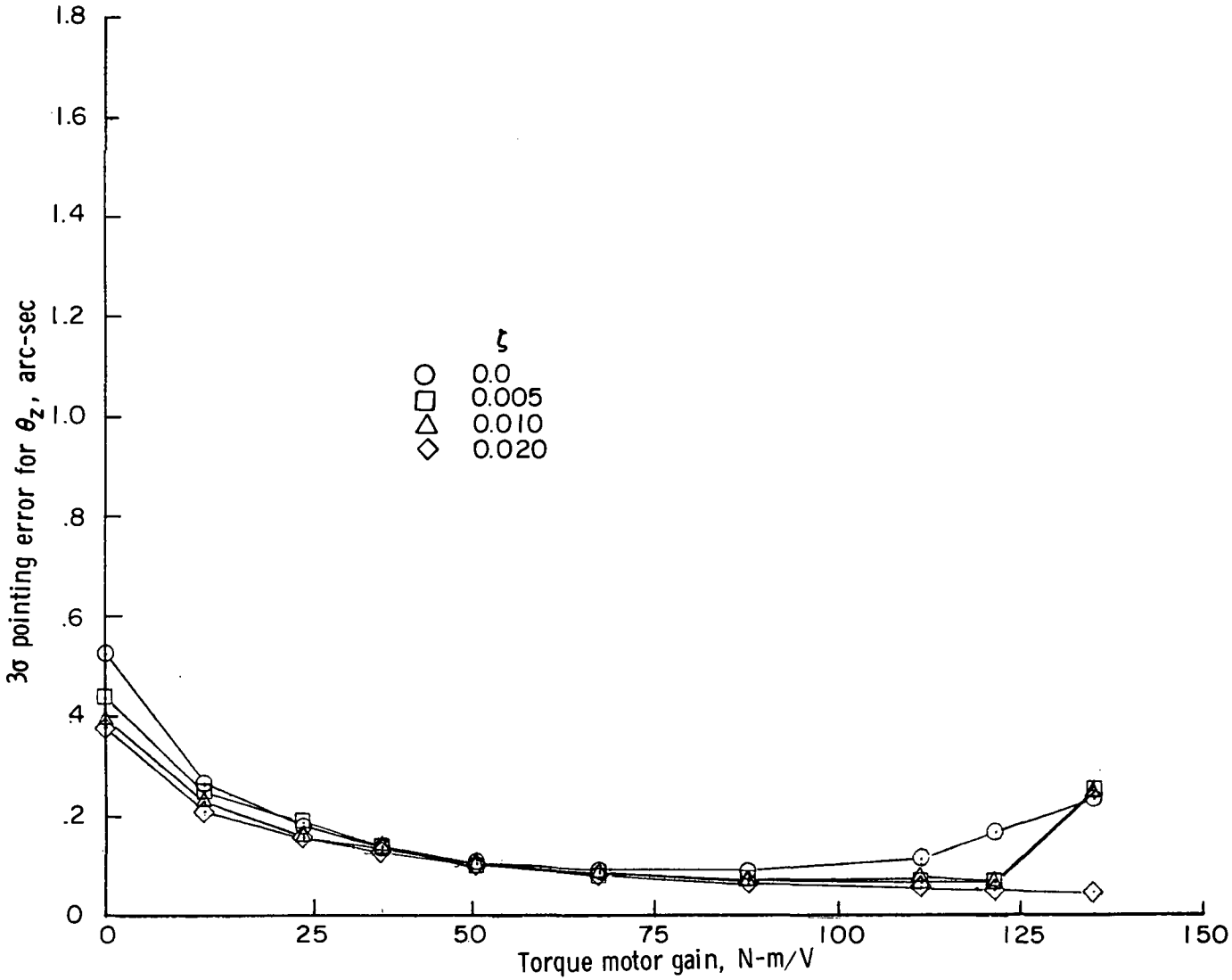

(b) Z_T-axis error.

Figure 5.- Concluded.

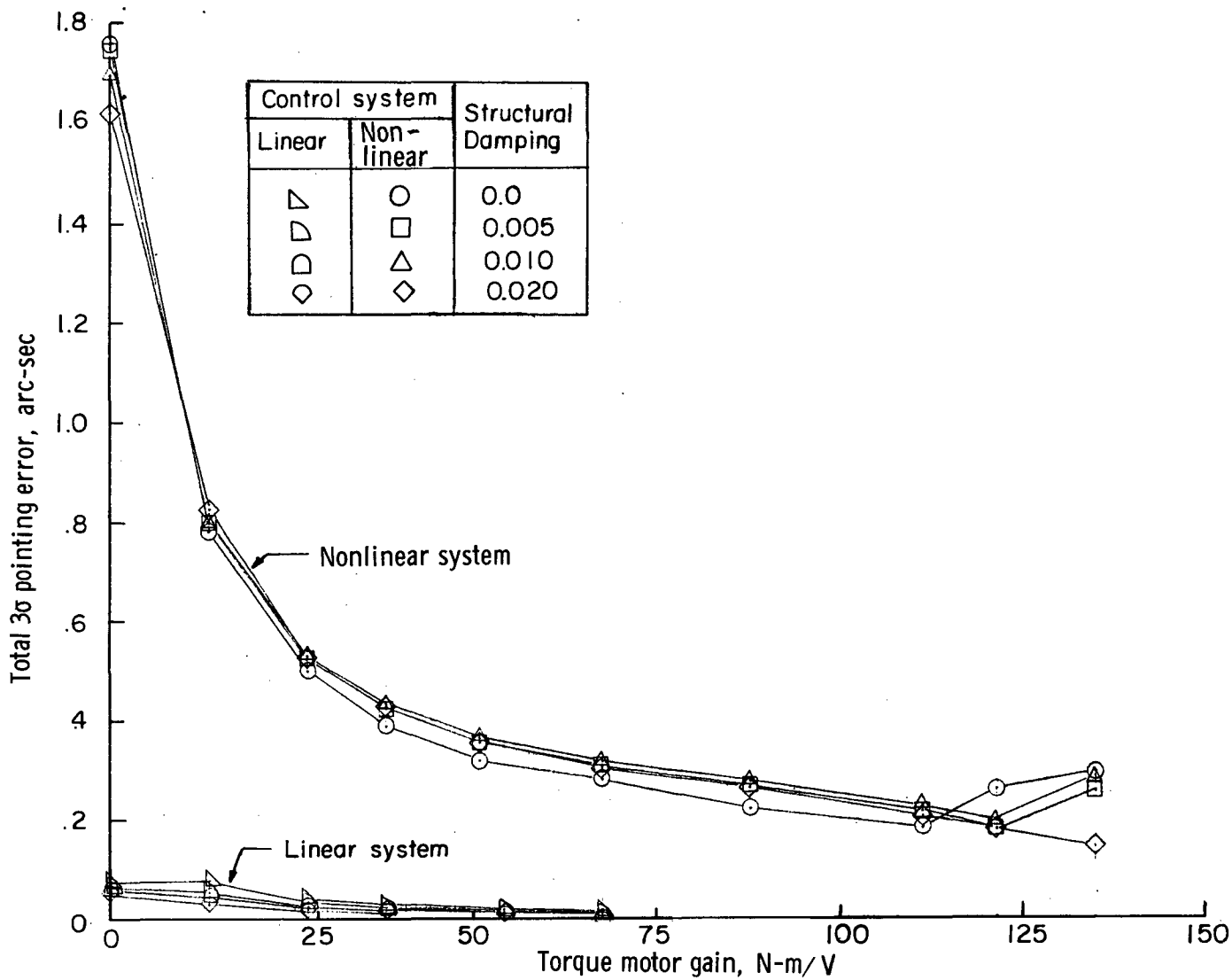

Figure 6.- Total linear- and nonlinear-system pointing-error variation with torque motor gain.

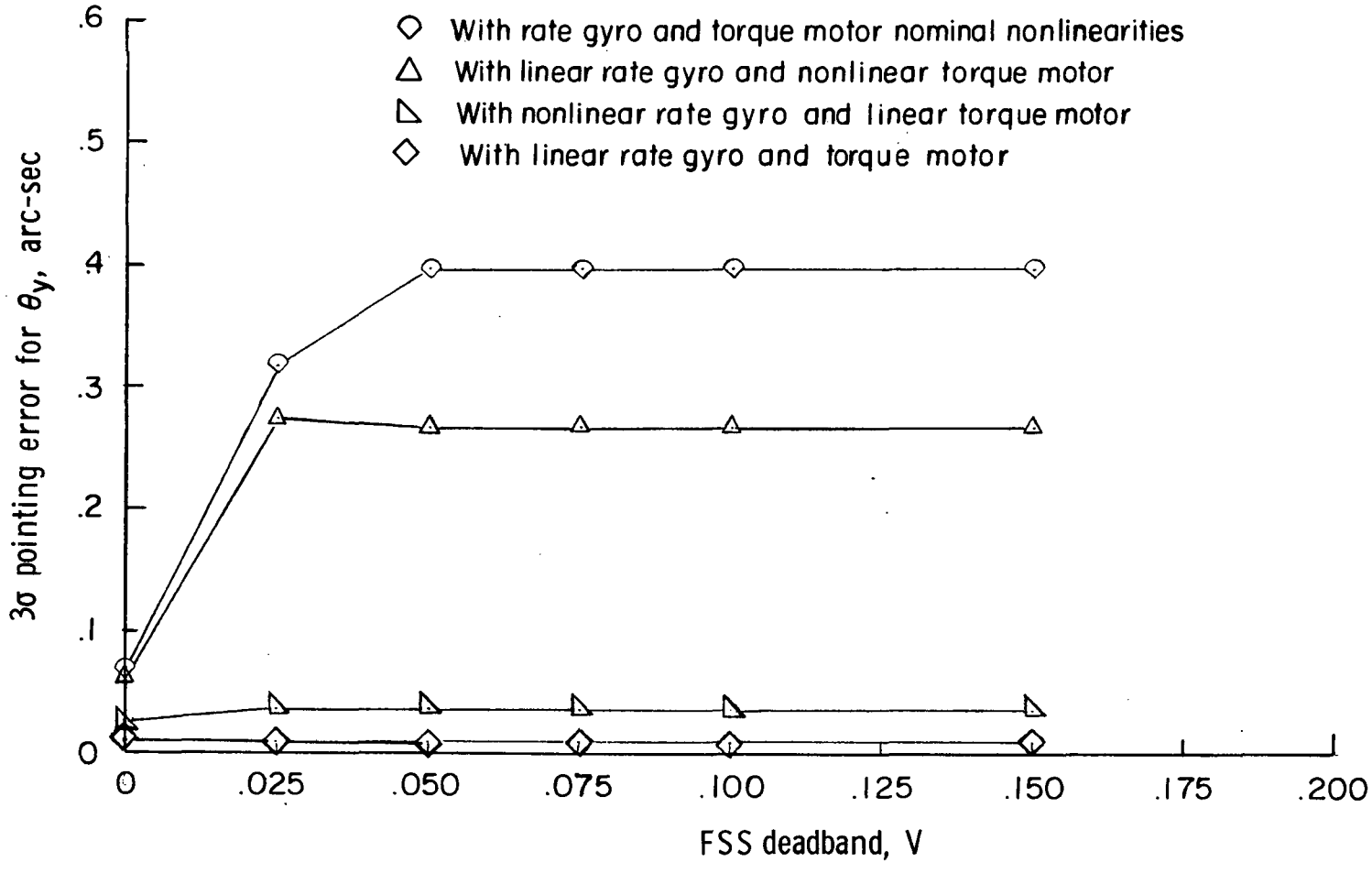

(a) Y_T-axis error.

Figure 7.- Variation of pointing error with sun-sensor deadband.

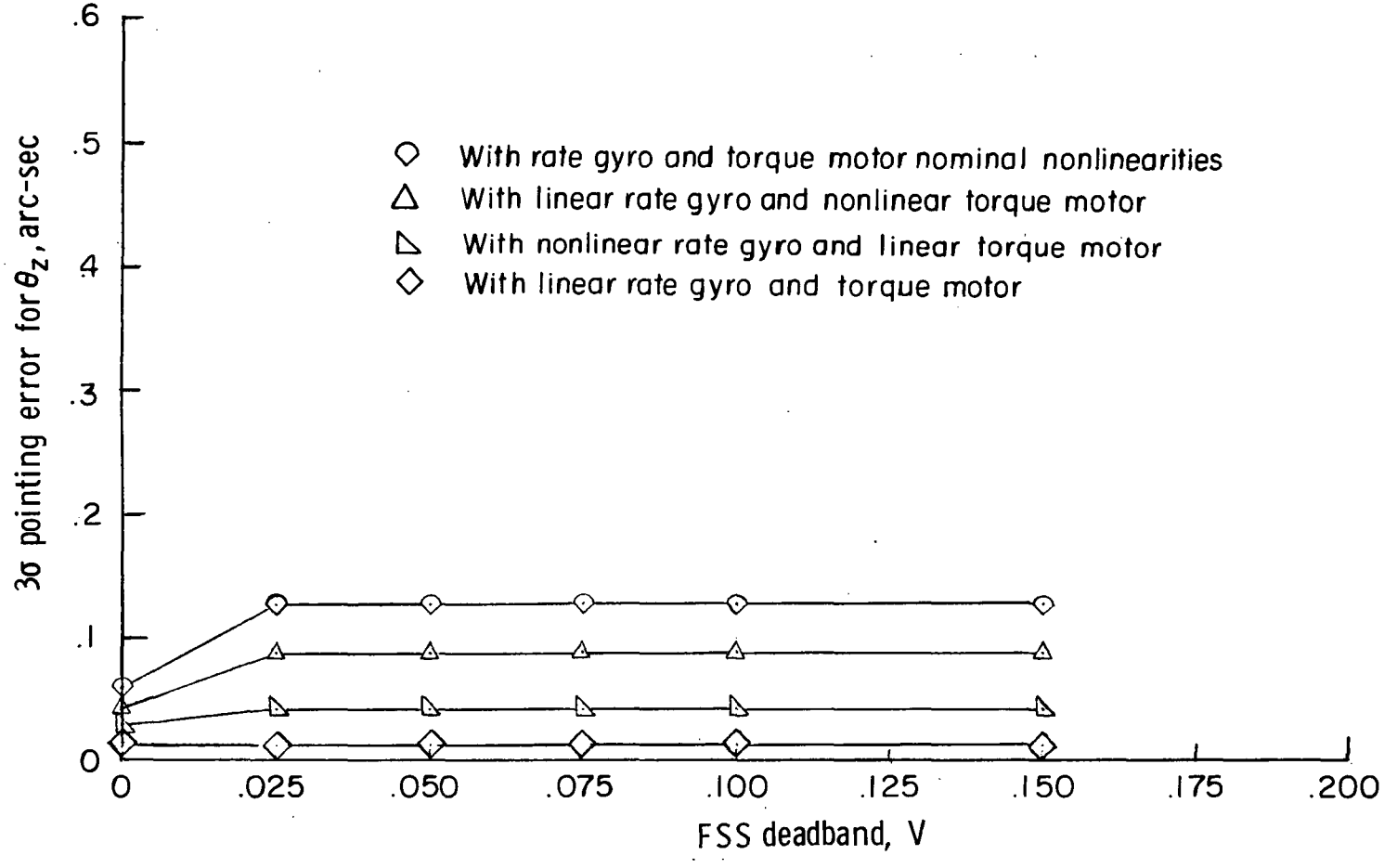

(b) Z_T-axis error.

Figure 7.- Continued.

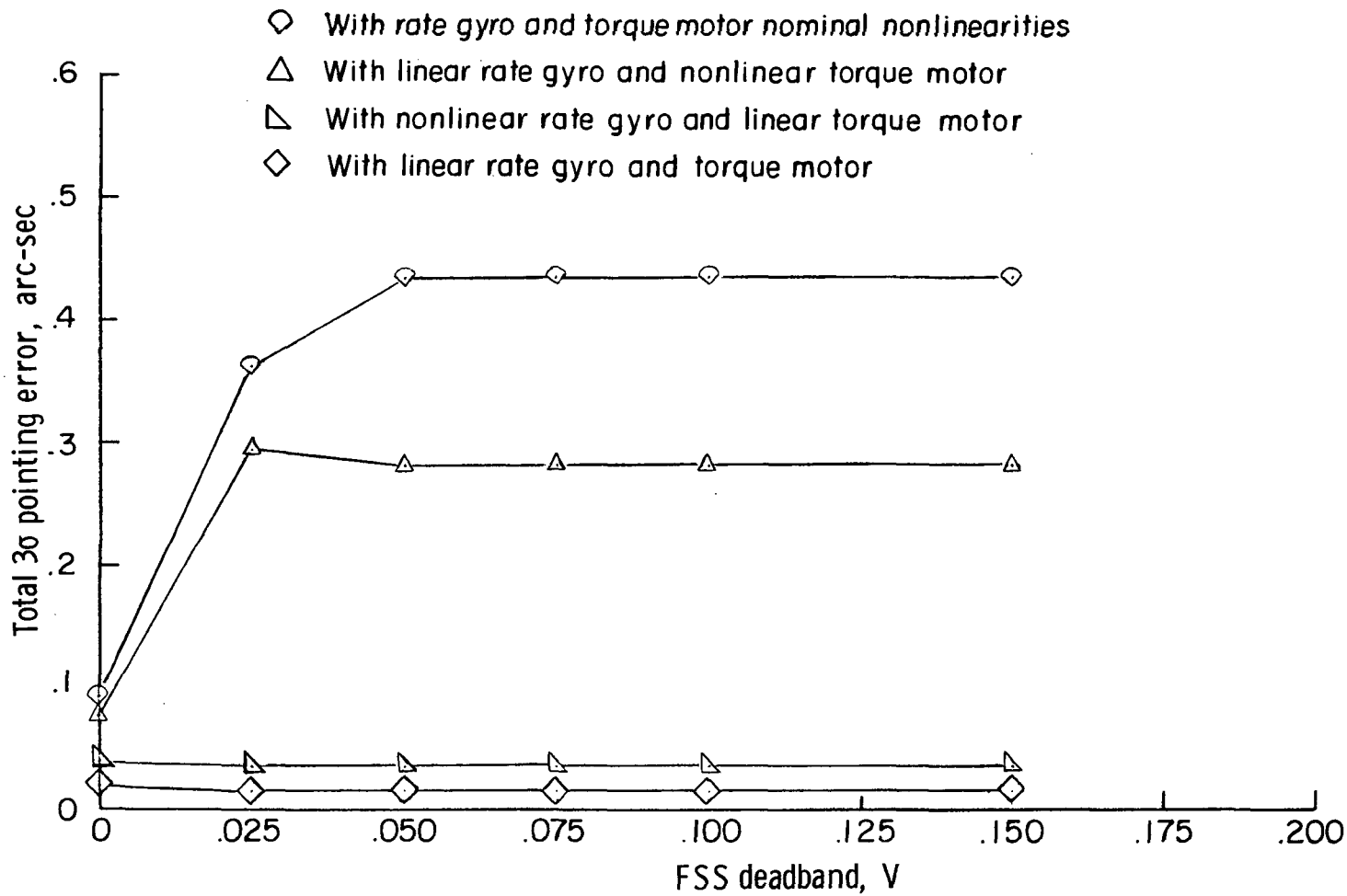

(c) Total pointing error.

Figure 7.- Concluded.

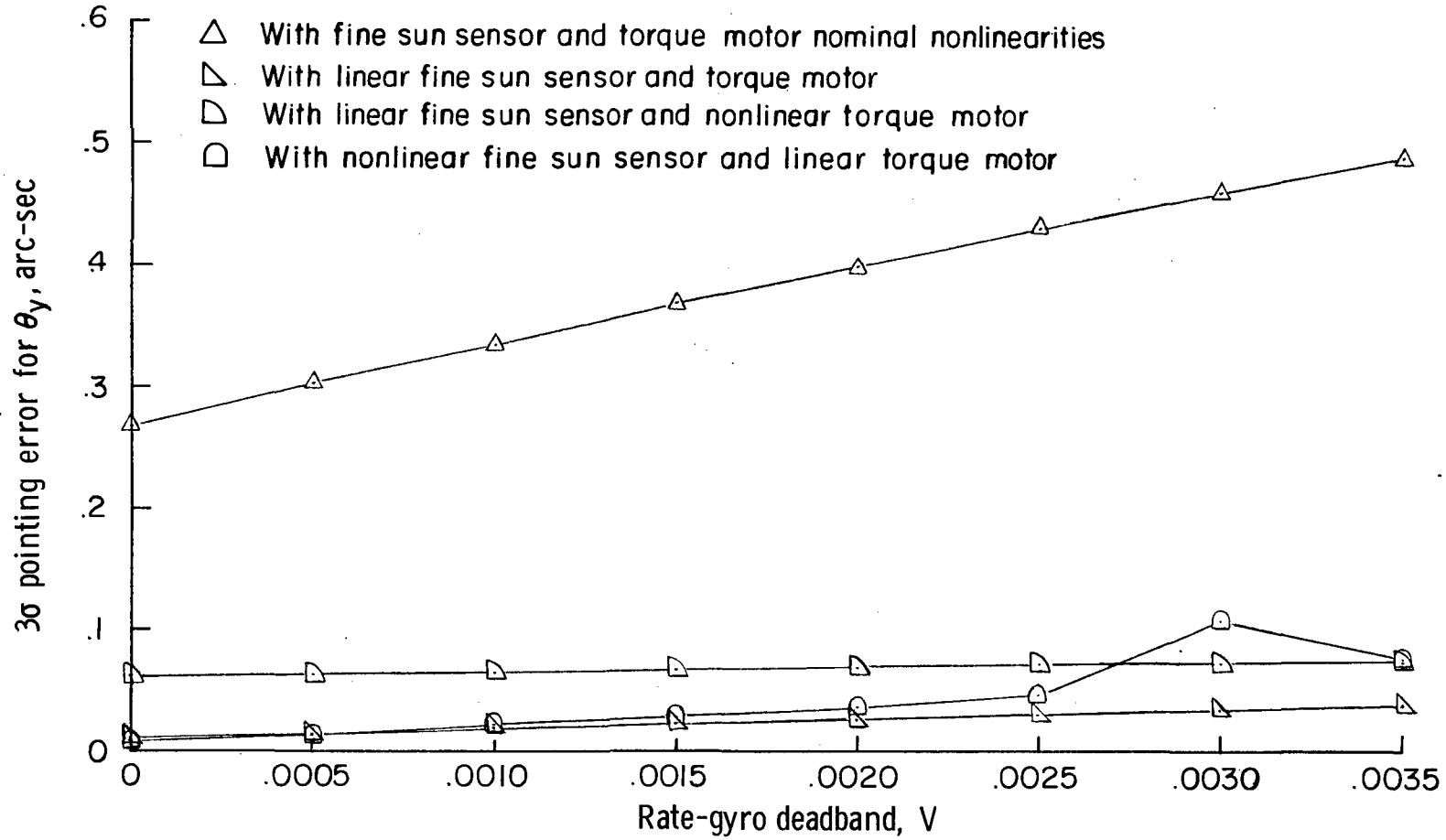

(a) Y_T-axis error.

Figure 8.- Variation of pointing error with rate-gyro deadband.

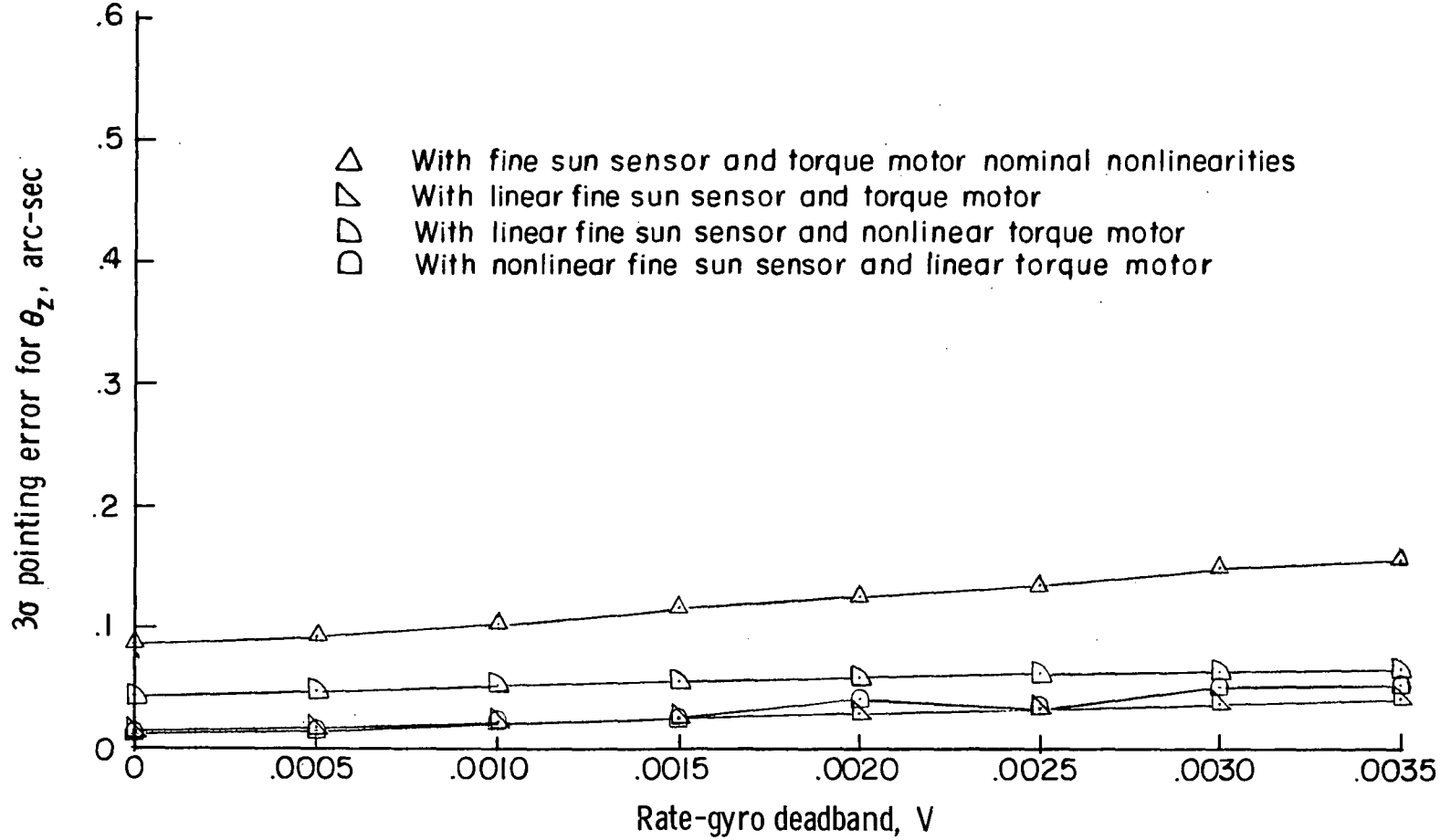

(b) Z_T-axis error.

Figure 8.- Continued.

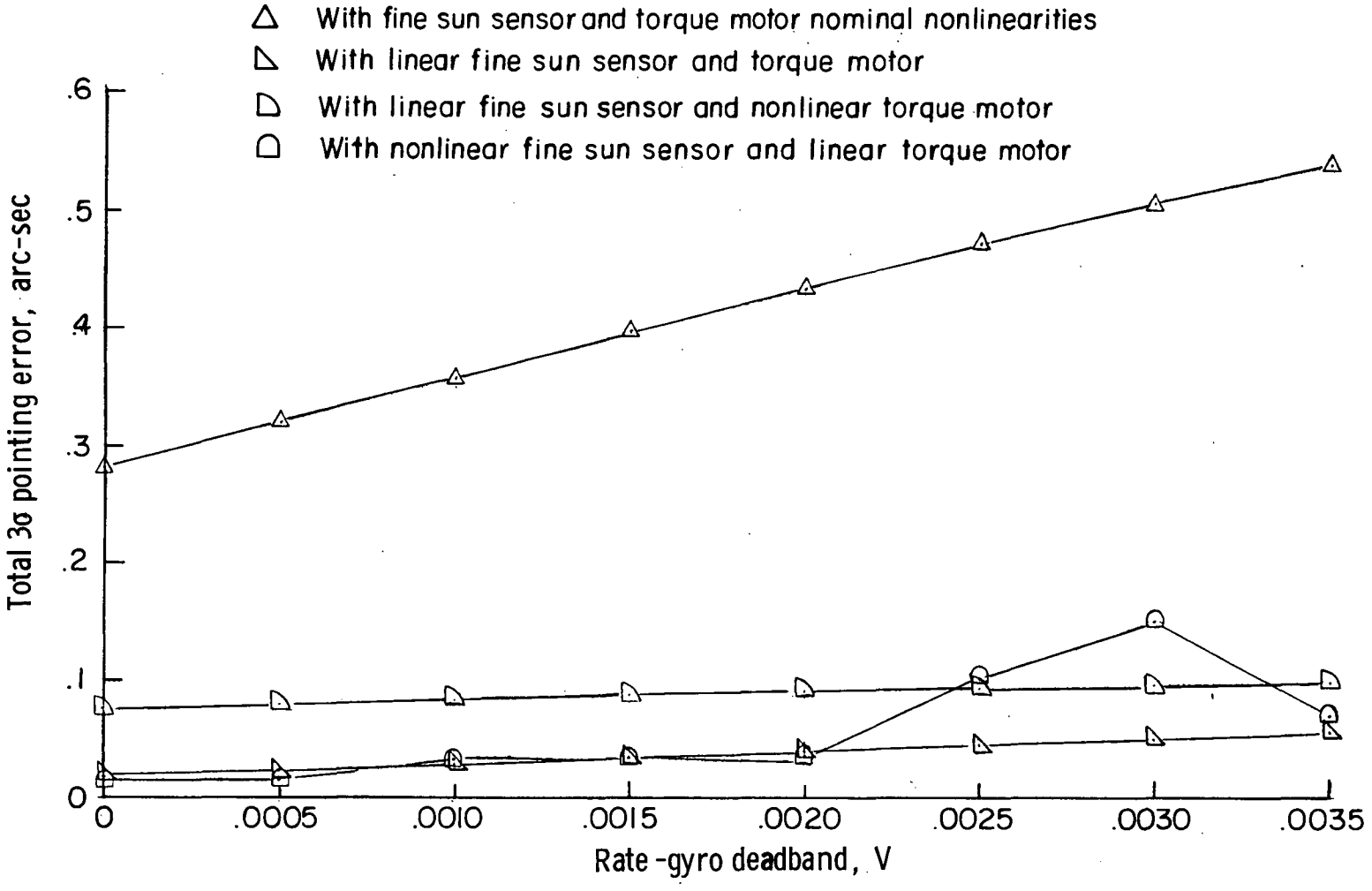

(c) Total error.

Figure 8.- Concluded.

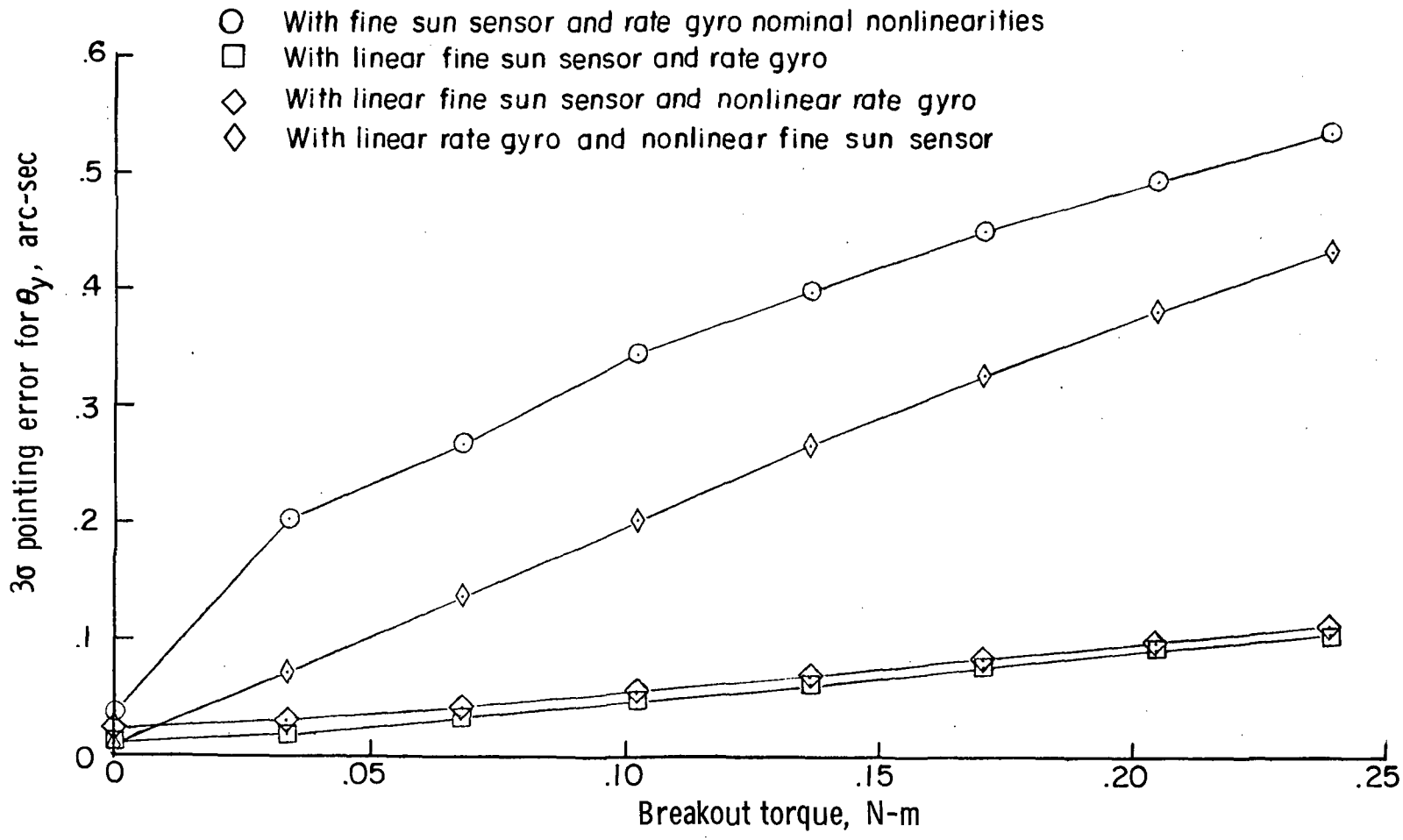

(a) Y_T-axis error.

Figure 9.- Variation of pointing error with torque motor breakout.

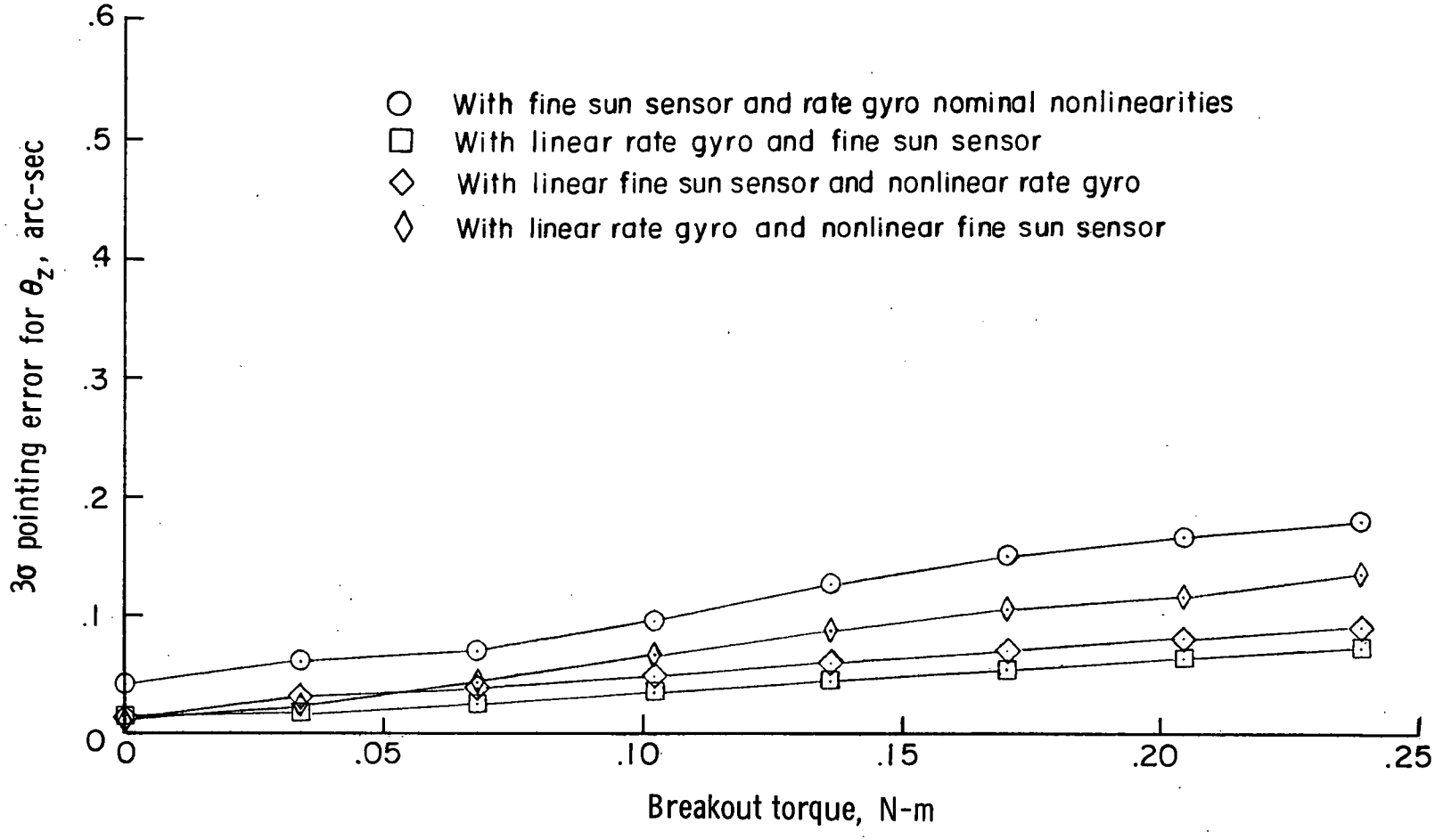

(b) Z_T-axis error.

Figure 9.- Continued.

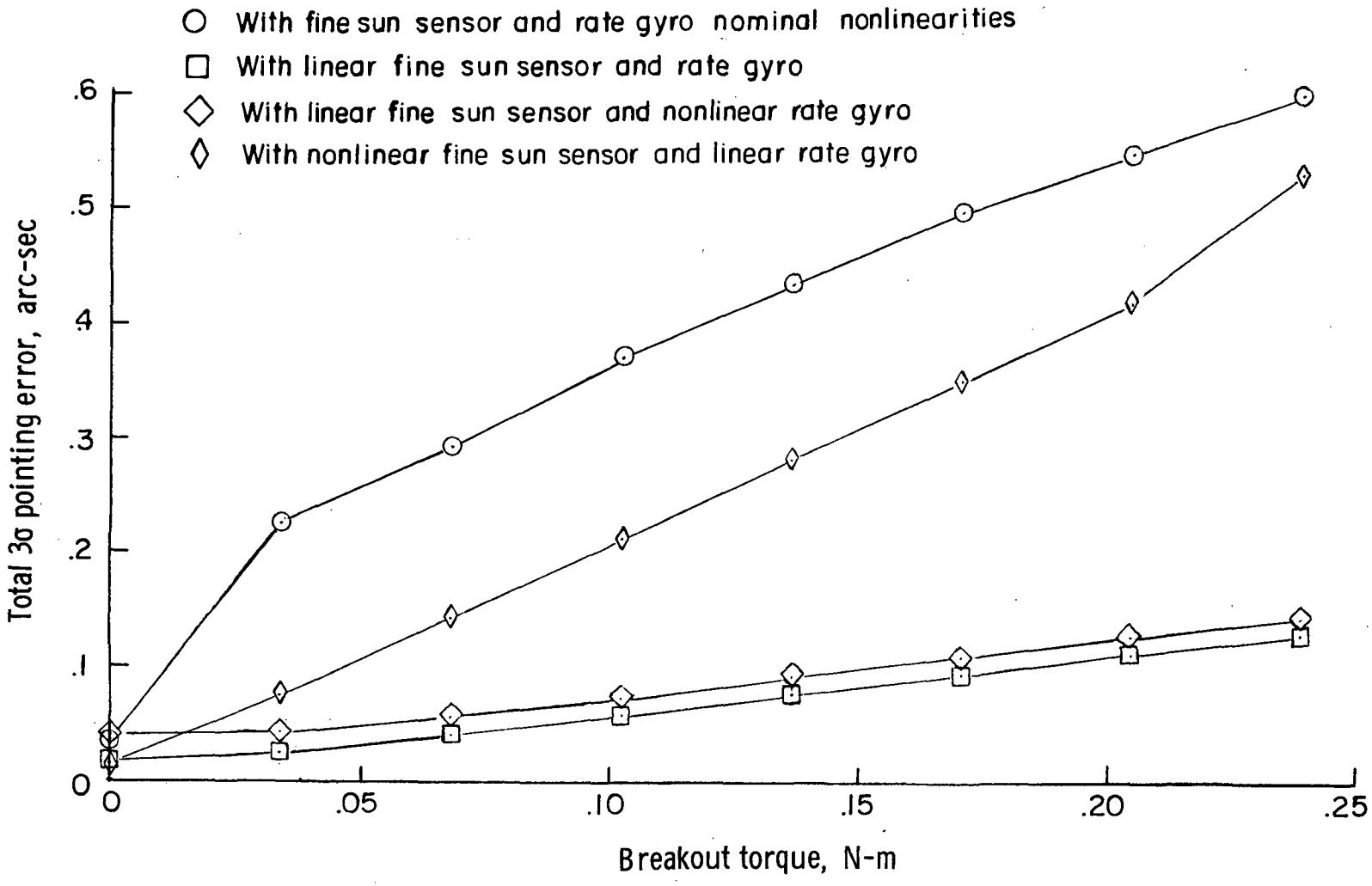

(c) Total error.

Figure 9.- Concluded.

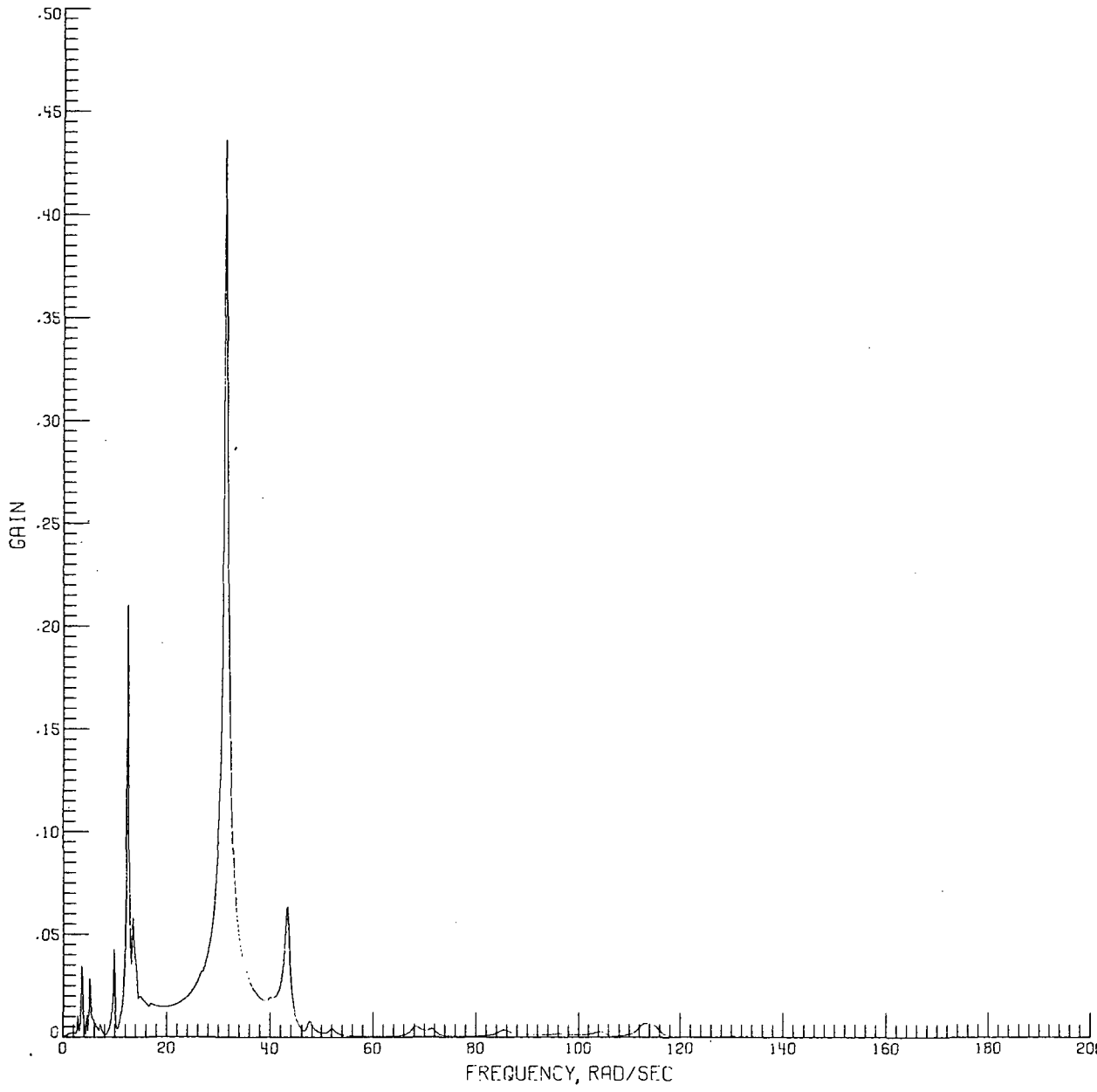

(a) Input at crew-motion filters and output at Y_T-axis sun-sensor location.

Figure 10.- Variation of relative gain with frequency for the linear system with complete modal data.

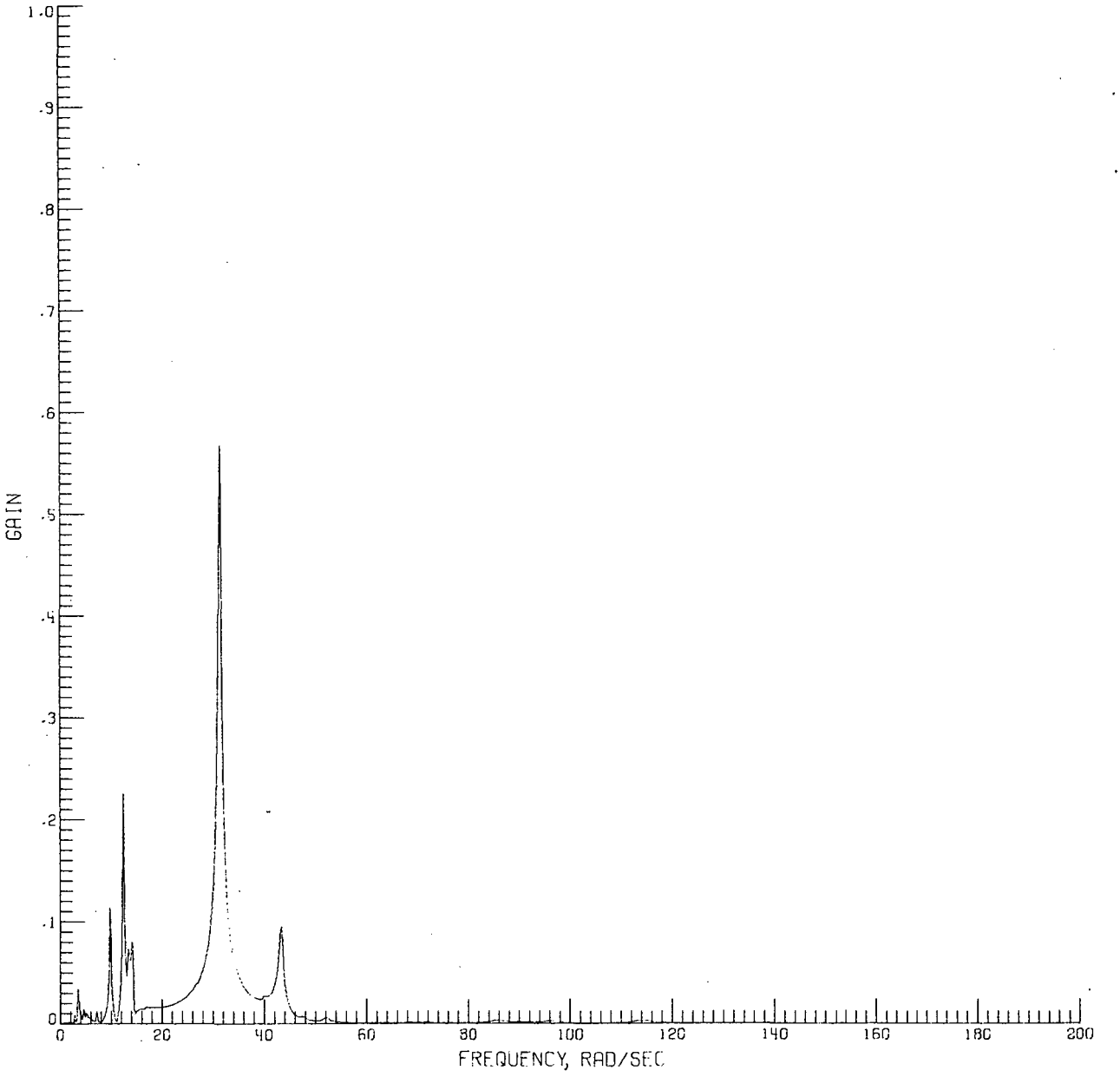

(b) Input at crew-motion filters and output at Z_T-axis rate-gyro location.

Figure 10.- Continued.

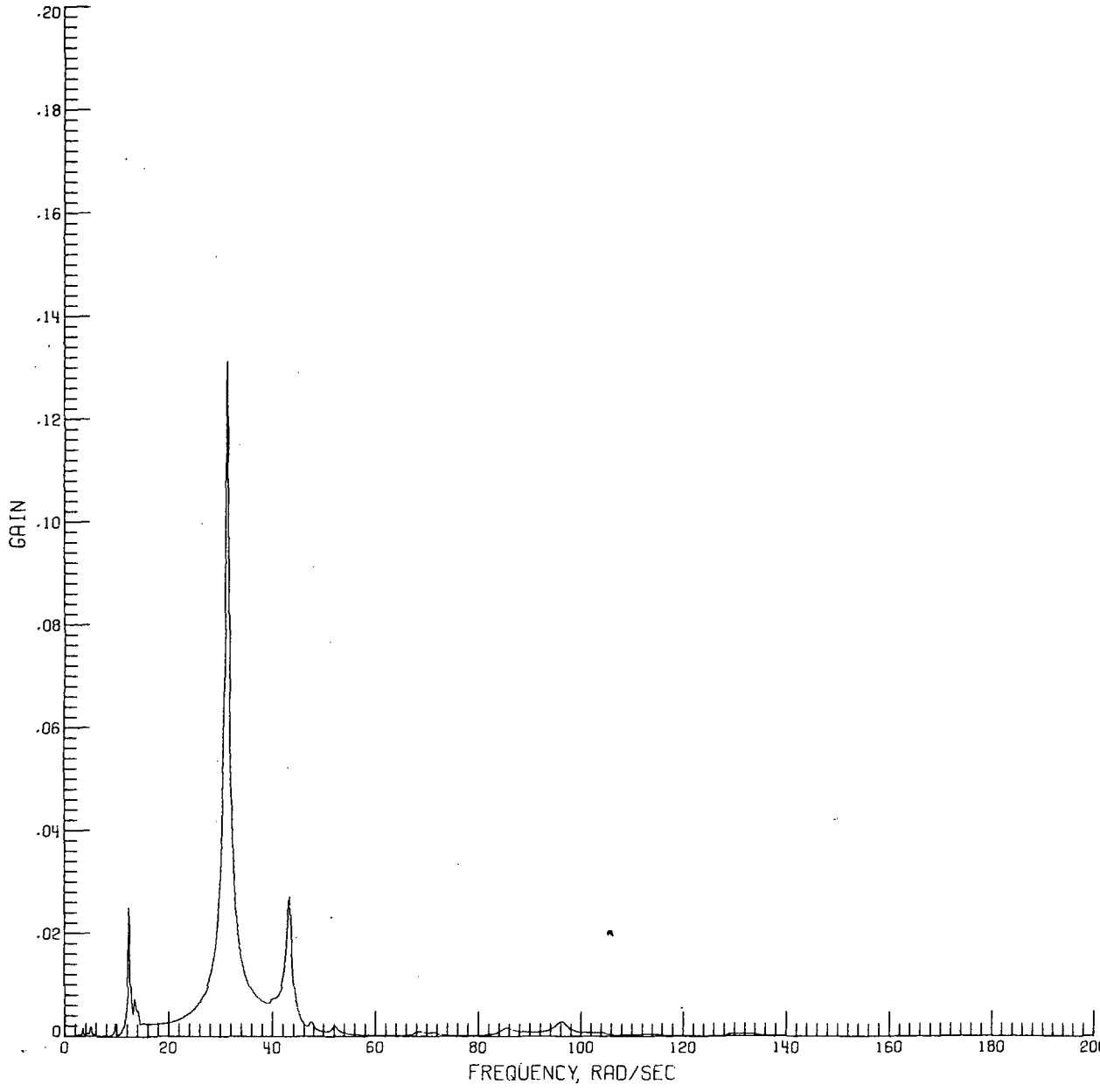

(c) Input at crew-motion filters and output at Y_T-axis rate-gyro location.

Figure 10.- Continued.

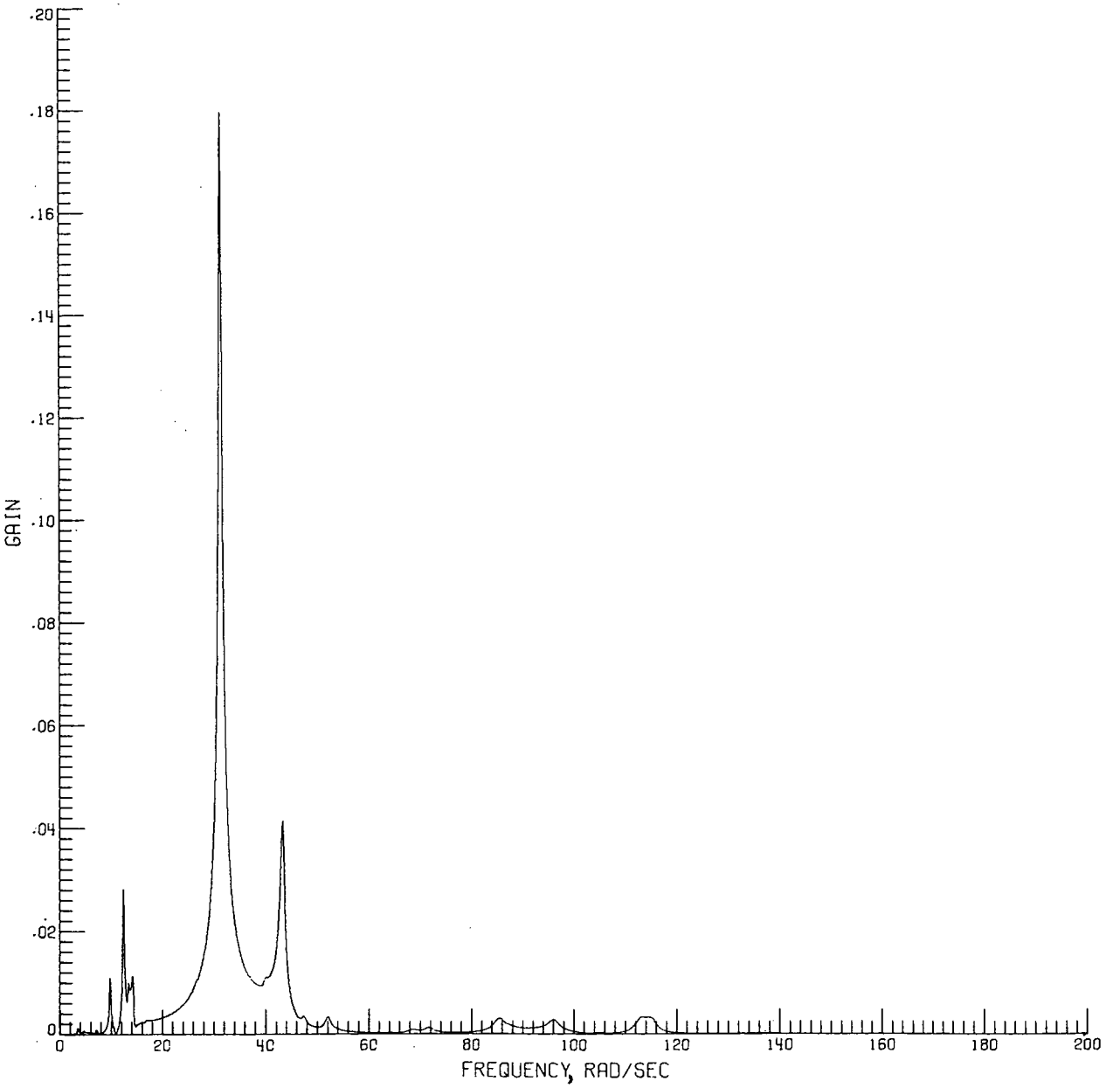

(d) Input at crew-motion filters and output at Z_T-axis rate-gyro location.

Figure 10.- Concluded.

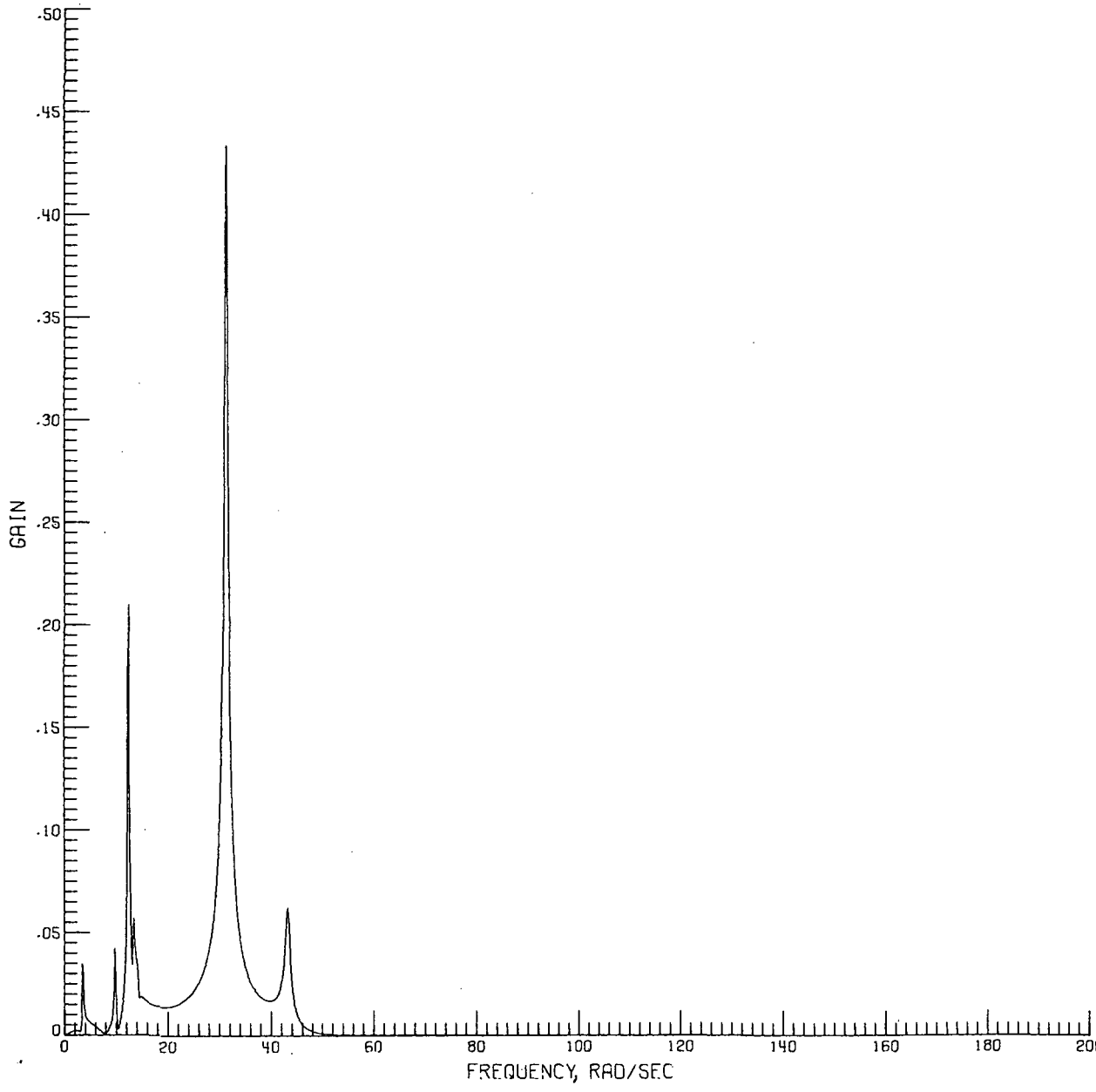

(a) Input at crew-motion filters and output at Y_T-axis sun-sensor location.

Figure 11.- Variation of relative gain with frequency for the linear system with truncated modal data.

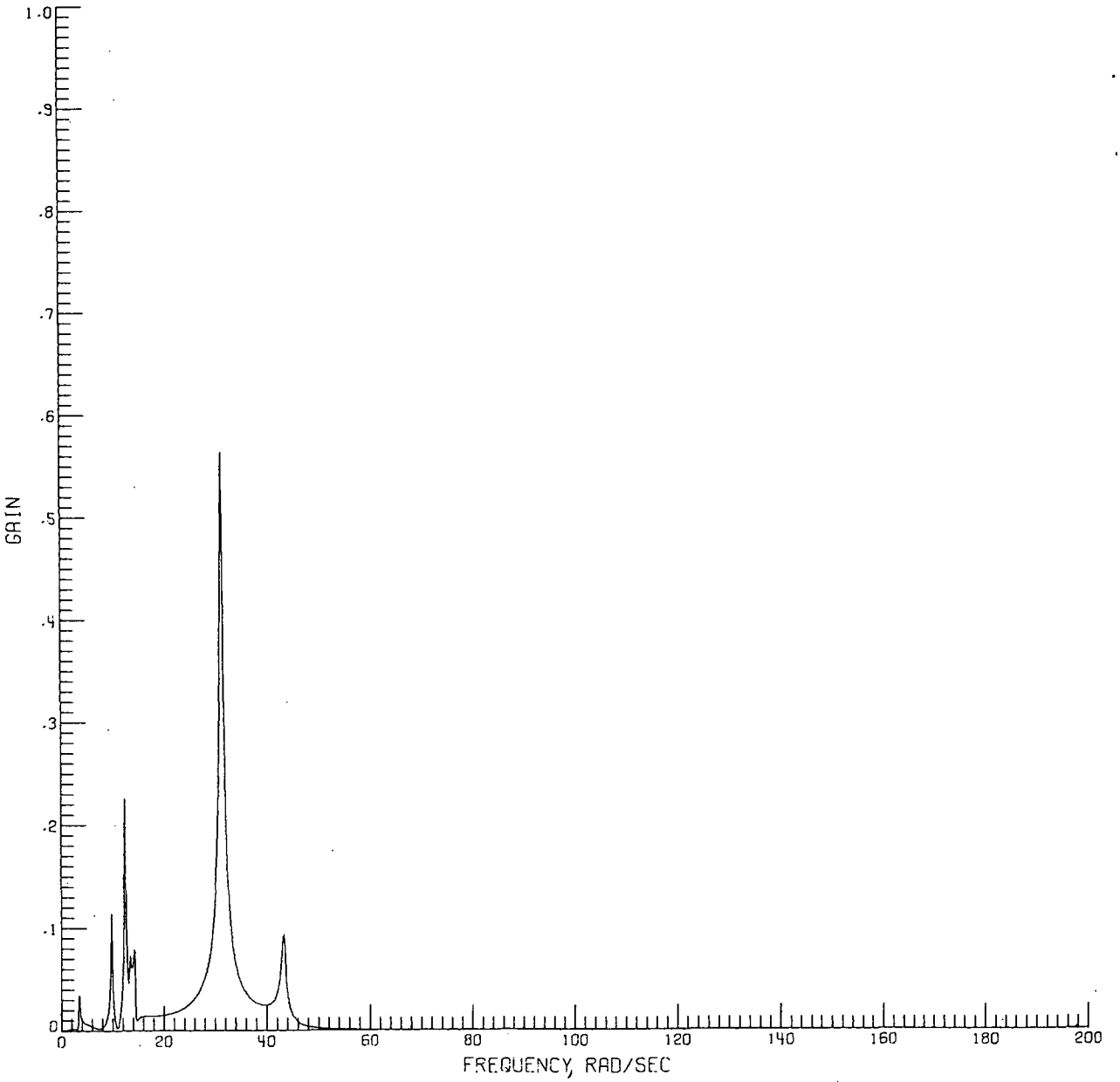

(b) Input at crew-motion filters and output at Z_T-axis sun-sensor location.

Figure 11.- Continued.

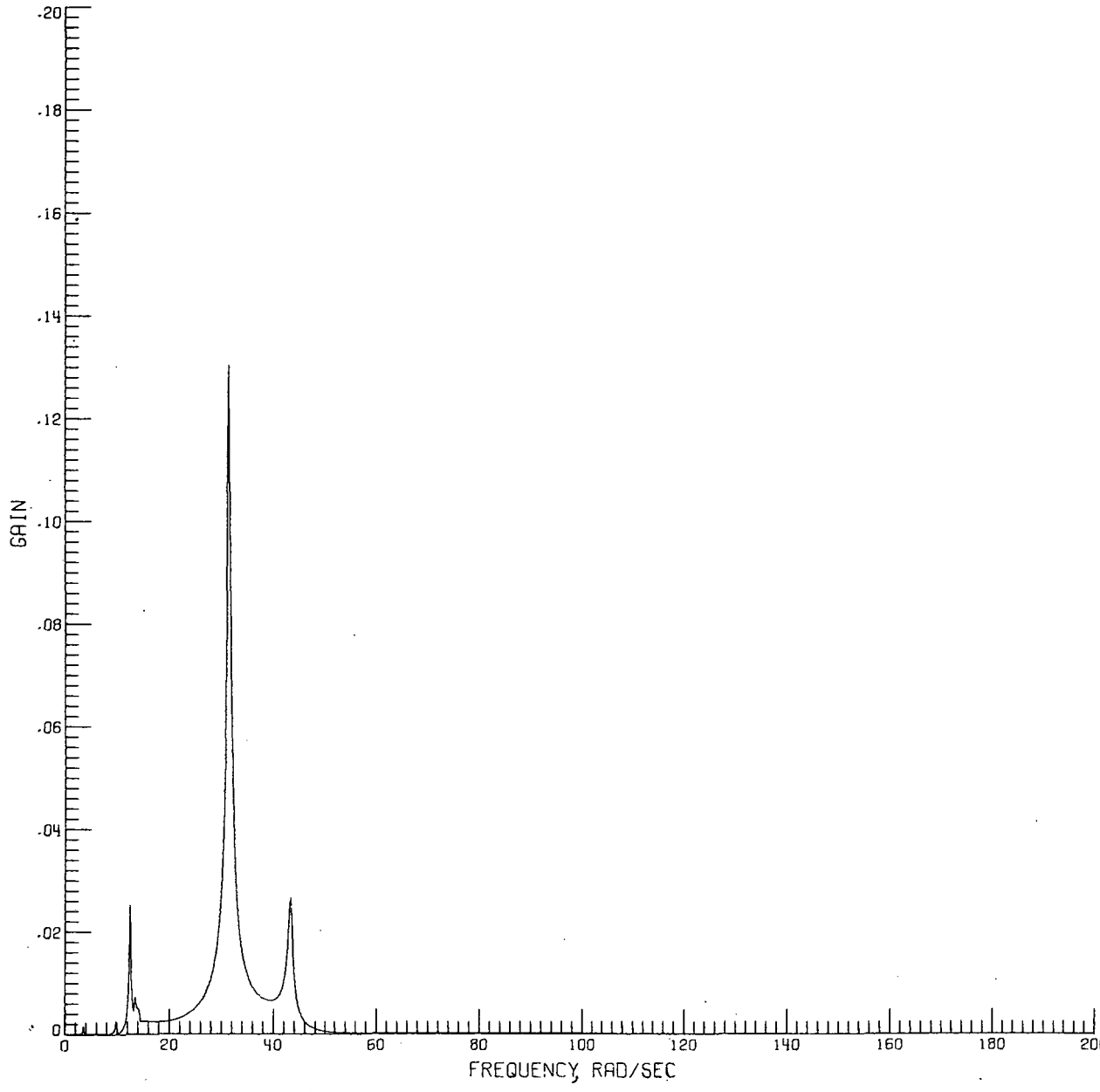

(c) Input at crew-motion filters and output at Y_T-axis rate-gyro location.

Figure 11.- Continued.

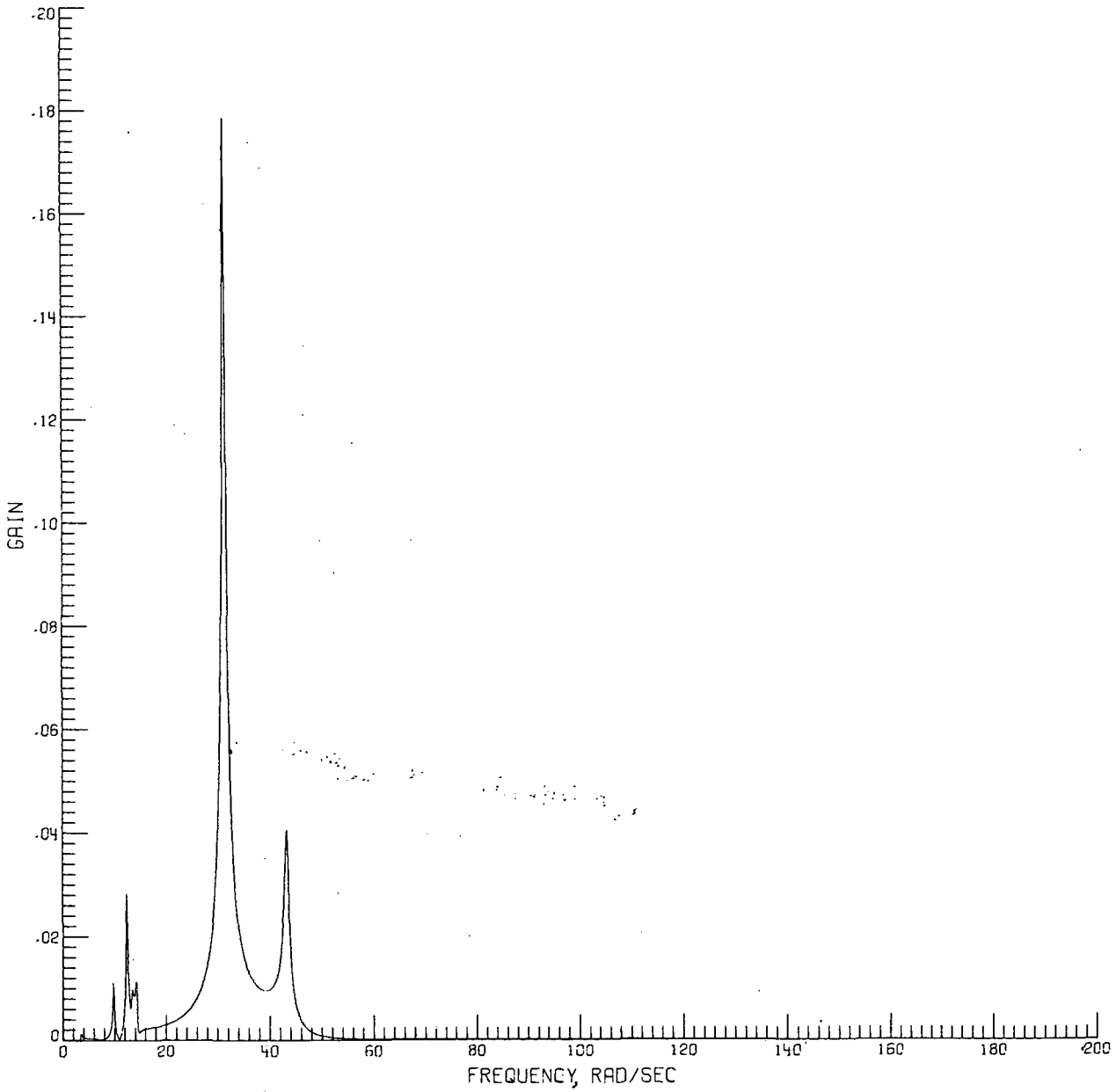

(d) Input at crew-motion filters and output at Z_T-axis rate-gyro location.

Figure 11.- Concluded.

Page Intentionally Left Blank

Page Intentionally Left Blank

NATIONAL AERONAUTICS AND SPACE ADMINISTRATION
WASHINGTON, D.C. 20546

OFFICIAL BUSINESS
PENALTY FOR PRIVATE USE $300

SPECIAL FOURTH-CLASS RATE BOOK

POSTAGE AND FEES PAID
NATIONAL AERONAUTICS AND SPACE ADMINISTRATION
451

U.S.MAIL

POSTMASTER: If Undeliverable (Section 158 Postal Manual) Do Not Return

"The aeronautical and space activities of the United States shall be conducted so as to contribute . . . to the expansion of human knowledge of phenomena in the atmosphere and space. The Administration shall provide for the widest practicable and appropriate dissemination of information concerning its activities and the results thereof."

—NATIONAL AERONAUTICS AND SPACE ACT OF 1958

NASA SCIENTIFIC AND TECHNICAL PUBLICATIONS

TECHNICAL REPORTS: Scientific and technical information considered important, complete, and a lasting contribution to existing knowledge.

TECHNICAL NOTES: Information less broad in scope but nevertheless of importance as a contribution to existing knowledge.

TECHNICAL MEMORANDUMS: Information receiving limited distribution because of preliminary data, security classification, or other reasons. Also includes conference proceedings with either limited or unlimited distribution.

CONTRACTOR REPORTS: Scientific and technical information generated under a NASA contract or grant and considered an important contribution to existing knowledge.

TECHNICAL TRANSLATIONS: Information published in a foreign language considered to merit NASA distribution in English.

SPECIAL PUBLICATIONS: Information derived from or of value to NASA activities. Publications include final reports of major projects, monographs, data compilations, handbooks, sourcebooks, and special bibliographies.

TECHNOLOGY UTILIZATION PUBLICATIONS: Information on technology used by NASA that may be of particular interest in commercial and other non-aerospace applications. Publications include Tech Briefs, Technology Utilization Reports and Technology Surveys.

Details on the availability of these publications may be obtained from:

SCIENTIFIC AND TECHNICAL INFORMATION OFFICE

NATIONAL AERONAUTICS AND SPACE ADMINISTRATION

Washington, D.C. 20546